N72-20760

Research Conducted Under

NASA Grant No. NGL 11-002-083

APPLICATION OF THE GALERKIN METHOD IN THE DESIGN OF STABLE LIQUID ROCKET MOTORS

SEMIANNUAL REPORT COVERING PERIOD

August 1, 1971 - January 31, 1972

Prepared By

Ben T. Zinn, Professor

Eugene A. Powell, Instructor

Manuel E. Lores, Graduate Research Assistant

S. Kalyanasundaram, Graduate Research Assistant

GEORGIA INSTITUTE OF TECHNOLOGY

SCHOOL OF AEROSPACE ENGINEERING

ATLANTA, GEORGIA

Project Monitor: Dr. Richard J. Priem

INTRODUCTION

During the period covered by this report work continued in the following three areas: (1) the development of the third-order, multi-mode theory to study the behavior of large amplitude transverse instabilities, (2) the study of nonlinear axial mode instability, and (3) the study of the influence of the functional form of the unsteady combustion response function upon the stability characteristics of rocket motors. Also a study was begun to improve the second order potential theory in order to provide a better approximation to the nozzle boundary condition.

The following papers were presented during this report period:

(1) "Application of the Galerkin Method to the Solution of Non-Linear Axial Combustion Instability Problems in Liquid Rockets," co-authored by B. T. Zinn and M. E. Lores and presented at the Third International Colloquium on Gasdynamics of Explosions and Reactive Systems in Marseille, France.

(2) "A Third Order, Single Mode Analysis of the Stability of Liquid-Propellant Rocket Motors," co-authored by E. A. Powell and B. T. Zinn and presented at the 8th JANNAF Liquid Propellant Combustion Instability Meeting in Los Angeles.

(3) "Application of the Galerkin Method in the Solution of Nonlinear Axial Instability in Liquid Rockets," co-authored by B. T. Zinn and M. E. Lores and presented at the 8th JANNAF Liquid Propellant Combustion Instability Meeting in Los Angeles.

A brief description of results obtained in the above-mentioned investigations is provided in the following sections.

SECOND ORDER INVESTIGATIONS

Three Dimensional Potential Theory

During the first phase of this research program a second order potential theory using the n-τ combustion model was developed[1]. This theory was restricted to two-dimensional (pure transverse) modes of instability and to rocket motors using a multi-orifice (quasi-steady) nozzle. The approximate solutions were expressed in terms of the acoustic modes for a cylindrical chamber with solid wall boundary conditions at both the injector and the nozzle ends. Consequently the approximation of the flow conditions at the nozzle entrance was relatively poor.

A study was begun to improve the second order potential theory by choosing a series expansion for the velocity potential that provides a better approximation to the flow at the nozzle entrance. This was done by expanding the velocity potential in terms of the acoustic eigenfunctions for a chamber with a solid wall boundary condition at the injector end and a nozzle admittance condition at the other end. This removes both the two-dimensionality and the quasi-steady nozzle restrictions of the previous theory.

Acoustic Eigenfunctions and Eigenvalues. The acoustic eigenfunctions and eigenvalues are determined by solving the acoustic wave equation:

$$\Phi_{rr} + \frac{1}{r}\Phi_r + \frac{1}{r^2}\Phi_{\theta\theta} + \Phi_{zz} - \Phi_{tt} = 0 \tag{1}$$

subject to the boundary conditions:

$$\begin{aligned} \Phi_r &= 0 \quad &&\text{at} \quad r = 1 \\ \Phi_z &= 0 \quad &&\text{at} \quad z = 0 \\ \Phi_z &= -\gamma Y \Phi_t \quad &&\text{at} \quad z = z_e \end{aligned} \tag{2}$$

In the above equations Φ is the velocity potential; r, θ, and z are the dimensionless radial, angular, and axial coordinates respectively; t is the dimensionless time; and γ is the specific heat ratio. The nozzle admittance, Y, is complex and is defined by:

$$Y = y_r + iy_i = (u'/p')_{z=z_e} \tag{3}$$

where u' is the dimensionless axial velocity perturbation and p' is the dimensionless pressure perturbation.

Using the method of separation of variables yields the following solution to Eqs. (1) and (2):

$$\Phi_{\ell mn} = \left\{F(t)\,Z_1(z) + G(t)\,Z_2(z)\right\} \Theta(\theta)R(r) \tag{4}$$

where

$$\begin{aligned} Z_1(z) &= \cos\left(\epsilon_{\ell mn} z\right)\cosh\left(\eta_{\ell mn} z\right) \\ Z_2(z) &= \sin\left(\epsilon_{\ell mn} z\right)\sinh\left(\eta_{\ell mn} z\right) \end{aligned} \tag{5}$$

$$\Theta(\theta) = \cos m\theta \quad \text{or} \quad \sin m\theta \tag{6}$$

$$R(r) = J_m\left(S_{mn} r\right) \tag{7}$$

$$\begin{aligned} F(t) &= e^{-\Lambda t}[C \cos \omega t - D \sin \omega t] \\ G(t) &= e^{-\Lambda t}[D \cos \omega t + C \sin \omega t] \end{aligned} \tag{8}$$

In Eqs. (5) $\epsilon_{\ell mn}$ and $\eta_{\ell mn}$ are the real and imaginary parts of the complex eigenvalue $b_{\ell mn}$, where ℓ, m, and n are the axial, tangential, and radial mode numbers, respectively. The functions $F(t)$ and $G(t)$ are seen to be damped sinusoids of equal amplitude and differing in phase by 90°. The frequency, ω, and damping, Λ, are related to the eigenvalues $\epsilon_{\ell mn}$, $\eta_{\ell mn}$, and S_{mn}; the frequency is very close to the frequency of a closed-ended chamber and the damping is small.

The eigenvalues $b_{\ell mn} = \epsilon_{\ell mn} + i\eta_{\ell mn}$ are the solutions of the following transcendental equation:

$$b_{\ell mn}^2 \sin^2\left(b_{\ell mn} z_e\right) + \gamma^2 Y^2\left(S_{mn}^2 + b_{\ell mn}^2\right)\cos^2\left(b_{\ell mn} z_e\right) = 0 \qquad (9)$$

A computer program has been developed to solve Eq. (9), and it has been used to determine the eigenvalues for quasi-steady nozzles $\left(y_r = \frac{\gamma-1}{2\gamma}\bar{u}_e,\ y_i = 0\right)$. The real part, $\epsilon_{\ell mn}$, is very close to $\ell\pi/z_e$, $\ell = 0,1,2,\ldots$, while the imaginary part, $\eta_{\ell mn}$, is a small positive number. Typical values are given in the following table for $\gamma = 1.2$, $z_e = 1.0$, and $\bar{u}_e = 0.2$ ($y_r = 0.01667$, $y_i = 0.0$).

Table 1. Acoustic Eigenvalues

ℓ	m	n	Mode	$\epsilon_{\ell mn}$	$\eta_{\ell mn}$
0	1	1	1T	0.1362	0.1352
1	1	1	1T-1L	3.1416	0.0232
2	1	1	1T-2L	6.2832	0.0209
0	2	1	2T	0.1763	0.1733
1	2	1	2T-1L	3.1417	0.0279
2	2	1	2T-2L	6.2832	0.0223

The axial acoustic eigenfunctions given by Eqs. (5) are plotted in Fig. 1 for the first tangential ($\ell = 0$, m = 1, n = 1) mode and the combined 1T-1L ($\ell = 1$, m = 1, n = 1) mode. Inspecting these curves and recalling that $p' = -\gamma\Phi_t$ and $u' = \Phi_z$ reveals that Z_1 is the greatest contributor to the pressure perturbation while Z_2 has the greatest influence on the axial velocity perturbation. This observation implies that in order to properly describe both pressure and axial velocity perturbations, both eigenfunctions must be included in the series expansion of the velocity potential.

Series Expansion. Based on the above remarks, the following series expansion is used in the three-dimensional nonlinear theory:

$$\tilde{\Phi} = \sum_{\ell}\sum_{m}\sum_{n} \Big\{\Big[A_{\ell mn}(t)\sin m\theta + B_{\ell mn}(t)\cos m\theta\Big]\cos\left(\epsilon_{\ell mn} z\right)\cosh\left(\eta_{\ell mn} z\right)$$

$$+ \Big[C_{\ell mn}(t)\sin m\theta + D_{\ell mn}(t)\cos m\theta\Big]\sin\left(\epsilon_{\ell mn} z\right)\sinh\left(\eta_{\ell mn} z\right)\Big\} J_m\left(S_{mn} r\right) \tag{10}$$

where both sin mθ and cos mθ are included in order to describe both standing and spinning waves. In order to simplify the algebra involved in applying the Galerkin Method, the expansion of the velocity potential is written as a single summation as follows:

$$\tilde{\Phi} = \sum_{p=1}^{N} A_p(t)\,\varphi_p(r,\theta,z) \tag{11}$$

where the A_p's are the unknown time-dependent coefficients and

$$\varphi_p(r,\theta,z) = \Theta_p(\theta)\,Z_p(z)\,R_p(r) \tag{12}$$

A correspondence must be established between the index, p, in Eq. (11) and the mode-numbers ℓ, m, and n in Eq. (10). In addition an integer S is needed to relate Eqs. (10) and (11). This relationship is given in the following table:

s(p)	$A_p(t)$	$\Theta_p(\theta)$	$Z_p(z)$	$R_p(r)$
1	$A_{\ell mn}(t)$	$\sin m\theta$	$\cos \epsilon_{\ell mn} z \cosh \eta_{\ell mn} z$	$J_m(S_{mn} r)$
2	$B_{\ell mn}(t)$	$\cos m\theta$	$\cos \epsilon_{\ell mn} z \cosh \eta_{\ell mn} z$	$J_m(S_{mn} r)$
3	$C_{\ell mn}(t)$	$\sin m\theta$	$\sin \epsilon_{\ell mn} z \sinh \eta_{\ell mn} z$	$J_m(S_{mn} r)$
4	$D_{\ell mn}(t)$	$\cos m\theta$	$\sin \epsilon_{\ell mn} z \sinh \eta_{\ell mn} z$	$J_m(S_{mn} r)$

Application of the Galerkin Method. The Galerkin method is used to determine the set of ordinary differential equations which describe the unknown time-dependent functions which appear in Eq. (11). Substituting the approximate solution (i.e., Eq. (11)) into the nonlinear wave equation (see Ref. 1) and the nozzle boundary condition yields the equation residual $E(\tilde{\Phi})$ and the boundary residual $B(\tilde{\Phi})$. The nozzle boundary residual involves the nozzle admittance, Y, which is a complex number, thus an equivalent formulation involving only real variables is needed. Thus $B(\tilde{\Phi})$ is expressed in the following form:

$$B(\tilde{\Phi}) = \left[\tilde{\Phi}_z + \gamma y_r \tilde{\Phi}_t + \gamma y_i \sum_{p=1}^{N} \frac{d^2 A_p}{dt^2} \frac{\varphi_p(r,\theta,z)}{\omega_p}\right]_{z=z_e} \qquad (13)$$

The residuals $E(\tilde{\Phi})$ and $B(\tilde{\Phi})$ must satisfy the following orthogonality conditions:

$$\int_0^{z_e}\int_0^{2\pi}\int_0^{1} E(\tilde{\Phi})\varphi_j(r,\theta,z)\, r\,dr\,d\theta\,dz - \int_0^{2\pi}\int_0^{1} B(\tilde{\Phi})\varphi_j(r,\theta,z_e)\, r\,dr\,d\theta = 0$$

$$j = 1,2,3,\ldots N \qquad (14)$$

Performing the spatial integrations indicated in Eqs. (14) yields the following system of differential equations to be solved for the A_p's:

$$\sum_{p=1}^{N}\left\{C_1(j,p)\frac{d^2A_p}{dt^2} + C_2(j,p)A_p(t) + \left[C_3(j,p) - nC_4(j,p)\right]\frac{dA_p}{dt}\right.$$

$$\left. + nC_4(j,p)\frac{d\left[A_p(t-\bar{\tau})\right]}{dt}\right\} + \sum_{p=1}^{N}\sum_{q=1}^{N}\left\{D(j,p,q)\, A_p \frac{dA_q}{dt}\right\} = 0$$

$$j = 1,2,3,\ldots N \qquad (15)$$

where the coefficients C_1, C_2, C_3, C_4, and D are functions of the spatial integrals involving Θ, Z, and R.

Computer Programs. A computer program, COEFFS, has been written to calculate the coefficients appearing in Eqs. (15). This program involves a number of subroutines whose functions are given below:

Subroutine	Function
UBAR	Calculates the steady state velocity distribution.
EIGVAL	Computes the axial acoustic eigenvalues $\epsilon_{\ell mn}$ and $\eta_{\ell mn}$.
FCNS	Evaluates certain functions needed by EIGVAL.
ZFUNCT	Calculates the axial eigenfunctions and their first and second derivatives (i.e., $Z_p(z)$, $Z_p'(z)$, and $Z_p''(z)$).
AXIAL1	Evaluates integrals involving products of two axial eigenfunctions.
AXIAL2	Evaluates integrals involving products of three axial eigenfunctions.
AZIMTL	Evaluates integrals involving products of three tangential eigenfunctions.
RADIAL	Evaluates integrals involving products of three radial eigenfunctions.
JBES	Evaluates Bessel functions needed by RADIAL.

The individual subroutines as well as the complete program, COEFFS, have been checked out and have been found to be functioning properly.

In order to numerically integrate Eqs. (15) they must be transformed to a form in which only one second derivative term appears in each equation. This decoupling process is accomplished by program COEFFS by computing the coefficients of the transformed equations using standard matrix inversion techniques. The resulting coefficients will be used as input to program LCYC3D, which numerically integrates the corresponding differential equations.

Program LCYC3D is currently under development. It is essentially a modified version of program LIMCYC of Ref. 1 and will be capable of calculating the transient behavior, limit-cycle amplitudes, and triggering amplitudes of three-dimensional instability in cylindrical rocket chambers with arbitrary nozzles.

Combustion Models

Work continued on the investigation of the influence of the functional form of the unsteady combustion response function upon the nonlinear stability characteristics of liquid-propellant rocket motors. This section describes the first phase of this study, in which the unsteady combustion mass source, W_m', is given by:

$$W_m' = \frac{d\bar{u}}{dz}\left[Ap' + B\,\frac{dp'}{dt}\right] \tag{16}$$

where A and B are prescribed constants, $\bar{u}$ is the steady state Mach number, and p' is the dimensionless pressure perturbation. The response function given by Eq. (16) is then incorporated into the second order potential theory of Ref. 1.

Analysis. Relating the pressure perturbation to the velocity potential and using a cylindrical coordinate system, Eq. (16) yields:

$$\begin{aligned} W_m' = -\gamma\,\frac{d\bar{u}}{dz}\Big\{A\Big[\Phi_t + \frac{1}{2}\Big(\Phi_r^2 + \frac{1}{r^2}\Phi_\theta^2 - \Phi_t^2\Big)\Big] \\ + B\Big[\Phi_{tt} + \Phi_r\Phi_{rt} + \frac{1}{r^2}\Phi_\theta\Phi_{\theta t} - \Phi_t\Big(\Phi_{rr} + \frac{1}{r}\Phi_r + \frac{1}{r^2}\Phi_{\theta\theta}\Big)\Big]\Big\} \end{aligned} \tag{17}$$

where only pure transverse (two-dimensional) solutions are considered. Introducing Eq. (17) into the nonlinear wave equation of Ref. 1 yields:

$$E(\Phi) = \Phi_{rr} + \frac{1}{r}\Phi_r + \frac{1}{r^2}\Phi_{\theta\theta} - \left(1 - \gamma B\frac{d\bar{u}}{dz}\right)\Phi_{tt}$$

$$- \left(2 - \gamma B\frac{d\bar{u}}{dz}\right)\left[\Phi_r\Phi_{rt} + \frac{1}{r^2}\Phi_\theta\Phi_{\theta t}\right]$$

$$- \left[\gamma\left(1 + B\frac{d\bar{u}}{dz}\right) - 1\right]\Phi_t\left(\Phi_{rr} + \frac{1}{r}\Phi_r + \frac{1}{r^2}\Phi_{\theta\theta}\right)$$

$$- \gamma\frac{d\bar{u}}{dz}(1-A)\ \Phi_t + \frac{\gamma A}{2}\frac{d\bar{u}}{dz}\left(\Phi_r^2 + \frac{1}{r^2}\Phi_\theta^2 - \Phi_t^2\right) = 0 \qquad (18)$$

which is restricted to combustors with small Mach number mean flow and moderate amplitude waves. For quasi-steady nozzles the nozzle boundary condition is given by:

$$B(\Phi) = \left[\frac{\gamma-1}{2}\bar{u}_e\Phi_t + \Phi_z\right]_{z=z_e} = 0 \qquad (19)$$

Approximate solutions to Eqs. (18) and (19) are obtained by means of the Method of Weighted Residuals. Restricting attention to pure transverse modes the velocity potential is expanded in terms of the acoustic eigenfunctions as follows:

$$\tilde{\Phi} = \sum_{m=0}^{M}\sum_{n=1}^{N}\left[A_{mn}(t)\sin m\theta + B_{mn}(t)\cos m\theta\right]J_m\left(S_{mn}r\right) \qquad (20)$$

where $A_{mn}(t)$ and $B_{mn}(t)$ are unknown functions of time. The assumed series expansion, Eq. (20), is introduced into Eqs. (18) and (19) to obtain the residuals $E(\tilde{\Phi})$ and $B(\tilde{\Phi})$, which are required to satisfy Galerkin orthogonality conditions similar to Eqs. (14). This process yields the following system of nonlinear, ordinary differential equations:

$$\left(1 - \frac{\gamma\bar{u}_e}{z_e} B\right) \frac{d^2 A_{jk}}{dt^2} + S_{jk}^2 A_{jk} + K \frac{dA_{jk}}{dt}$$

$$+ \sum_{m,n} \sum_{\mu,\nu} \left\{ C_1(m,n;\mu,\nu;j,k)\ A_{mn} \frac{dB_{\mu\nu}}{dt} + C_2(m,n;\mu,\nu;j,k)\ B_{mn} \frac{dA_{\mu\nu}}{dt} \right.$$

$$+ D_1(m,n;\mu,\nu;j,k)\ A_{mn}B_{\mu\nu} + D_2(m,n;\mu,\nu;j,k)\ B_{mn}A_{\mu\nu}$$

$$\left. + E_1(m,n;\mu,\nu;j,k)\ \frac{dA_{mn}}{dt} \frac{dB_{\mu\nu}}{dt} + E_2(m,n;\mu,\nu;j,k)\ \frac{dB_{mn}}{dt} \frac{dA_{\mu\nu}}{dt} \right\} = 0 \quad (21)$$

$$\left(1 - \frac{\gamma\bar{u}_e}{z_e} B\right) \frac{d^2 B_{jk}}{dt^2} + S_{jk}^2 B_{jk} + K \frac{dB_{jk}}{dt}$$

$$+ \sum_{m,n} \sum_{\mu,\nu} \left\{ C_3(m,n;\mu,\nu;j,k)\ A_{mn} \frac{dA_{\mu\nu}}{dt} + C_4(m,n;\mu,\nu;j,k)\ B_{mn} \frac{dB_{\mu\nu}}{dt} \right.$$

$$+ D_3(m,n;\mu,\nu;j,k)\ A_{mn}A_{\mu\nu} + D_4(m,n;\mu,\nu;j,k)\ B_{mn}B_{\mu\nu}$$

$$\left. + E_3(m,n;\mu,\nu;j,k)\ \frac{dA_{mn}}{dt} \frac{dA_{\mu\nu}}{dt} + E_4(m,n;\mu,\nu;j,k)\ \frac{dB_{mn}}{dt} \frac{dB_{\mu\nu}}{dt} \right\} = 0 \quad (22)$$

where

$$K = \frac{\gamma\bar{u}_e}{z_e} \left(1 + \frac{\gamma-1}{2\gamma} - A\right) \quad (23)$$

The coefficients of the nonlinear terms (i.e., C_i, D_i, and E_i for $i = 1,\ldots4$) are determined by evaluating the various integrals of trigonometric and Bessel functions that arise from the spatial integrations required by the Galerkin method. These coefficients depend on the combustion parameters A and B.

The unstable behavior of an engine is determined by specifying the form of the initial disturbance and then following the subsequent behavior of the individual modes (i.e., the functions $A_{jk}(t)$ and $B_{jk}(t)$) by numerically integrating Eqs. (21) and (22). Typical numerical solutions of these equations will be presented and discussed in the following paragraphs.

Linear Solutions. The linear stability limit is determined by substituting $B_{jk}(t) = be^{i\omega t}$ into Eq. (22) and neglecting the nonlinear terms. Separating real and imaginary parts in the resulting complex equation yields the following conditions for neutral stability:

$$A = 1 + \frac{\gamma-1}{2\gamma} \tag{24}$$

$$\omega = \frac{S_{jk}}{\sqrt{1 - \frac{\gamma\bar{u}_e}{z_e} B}} \tag{25}$$

The neutral stability limit and the stable and unstable regions are shown in the upper plot of Fig. 2. It is easily shown that for small amplitude (i.e., sinusoidal) oscillations the combustion response function given by Eq. (16) is equivalent to

$$W_m' = \frac{d\bar{u}}{dz}\left[Pe^{i\varphi}\right]p' \tag{26}$$

where P is the amplitude factor and φ is the phase shift. The lower plot of Fig. 2 shows how the stability map on the (A,B) plane transforms to the (P,φ) plane; the P-φ plot resembles an n-τ curve. In both plots the frequency increases as one moves to the right along the neutral stability curve.

The effects of chamber length, z_e, Mach number, $\bar{u}_e$, and the mode of oscillation on the linear stability limits are shown in

Figs. 3 and 4. These plots show that the neutral stability curves in both the (A,B) and (P,φ) planes are independent of $\bar{u}_e$, z_e, and S_{jk}. However the frequency corresponding to a given point on the (A,B) neutral stability curve does depend on these parameters; the frequency is proportional to S_{jk} and increases as the ratio $\bar{u}_e/z_e$ increases. Because of this frequency effect, the mapping of points from the (A,B) plane to the (P,φ) plane depends upon $\bar{u}_e/z_e$ and S_{jk} as shown in Figs. 3 and 4. These results indicate that the region of linear instability in the (A,B) plane is the same for all transverse modes.

The behavior of the linear solutions for points away from the (A,B) neutral stability limit is determined by assuming that $B_{jk}(t) = be^{(\Lambda+i\omega)t}$ and proceeding as before. In this manner the following expression is obtained for the growth rate, Λ:

$$\Lambda = \frac{\gamma\bar{u}_e/2z_e}{1 - \frac{\gamma\bar{u}_e}{z_e}B}\left[A - \left(1 + \frac{\gamma-1}{2\gamma}\right)\right] \tag{27}$$

From Eq. (27) lines of constant growth rate are determined as shown in the upper plot of Fig. 5. This plot shows that the growth (or decay) rate increases with increasing displacement above (or below) the neutral stability limit and with increasing B. A singular point occurs on the neutral stability limit at $B = z_e/\gamma\bar{u}_e$ where the constant-Λ lines intersect. Further analysis shows that oscillatory growth or decay can only occur for values of A and B lying to the left of the parabola shown in the lower plot of Fig. 5. Solutions for points above the parabola or for $B > z_e/\gamma\bar{u}_e$ exhibit non-oscillatory growth, while solutions below the parabola with $B < z_e/\gamma\bar{u}_e$ exhibit non-oscillatory decay.

<u>Nonlinear Solutions</u>. Nonlinear solutions were obtained with a three-mode series expansion consisting of the following acoustic modes: the first tangential (1T), the second tangential

(2T), and the first radial (1R) modes. All results presented in this section were obtained from a pure standing 1T initial disturbance of the form:

$$
\begin{aligned}
B_{11}(t) &= b_{11}\cos(1.84118t) \\
& \qquad\qquad\qquad\qquad\qquad t \leq 0 \qquad (28) \\
B_{21}(t) &= B_{01}(t) = 0
\end{aligned}
$$

Numerical solutions were obtained for values of A and B corresponding to the points shown in Fig. 6. These points represent conditions of linearly stable, neutral, and unstable oscillations. In each case the motor parameters were: $\gamma = 1.2$, $\bar{u}_e = 0.2$, and $L/D = 0.5$ (length-to-diameter ratio, $z_e/2$).

The first three cases (i.e., points a, b, and c of Fig. 6) were run to determine the transient behavior and the existence of limit-cycles for resonant combustion (i.e., $B = 0$ and $\omega = S_{11}$). The transient behavior is shown in Fig. 7 as plots of pressure perturbation, p', versus time. In each case the initial amplitude b_{11} was 0.2, and the calculations were terminated after 50 cycles. It is seen from Fig. 7 that the linearly stable case exhibits decay to zero amplitude, the neutrally stable case exhibits a slight growth, and the linearly unstable case exhibits slow growth initially followed by rapid growth after 40 cycles due to nonlinear coupling between unstable modes. The pressure peaks are seen to vary considerably in height, particularly for the linearly unstable case. It appears that if a limit-cycle is reached in the linearly unstable case, its amplitude will be too large to be described by the present second order theory.

The result described above is typical of results obtained with the (n,τ) model for regions of the (n,τ) plane for which all three modes in the series were linearly unstable. This result was expected since the region of linear instability in the (A,B) plane is the same for all modes.

Points a, d, and e in Fig. 6 were considered in order to investigate the possibility of triggering the 1T mode for both resonant and off-resonant conditions. In each case calculations were made for initial amplitudes b_{11} of 0.2, 0.5, 1.0, 2.0, and 5.0. Growth occurred only for amplitudes greater than about 2.0, thus triggering was only possible by the introduction of very large disturbance which violate the assumptions of the second order theory.

Two investigations concerning the (A,B) model are now in progress: (1) a comparison of the nonlinear growth or decay rates with those computed from linear theory (i.e., Eq. (27)) and (2) a study of the triggering characteristics of the 1R mode using a single mode series. Upon completion of these studies a complete evaluation of the (A,B) model will be made.

THIRD ORDER INVESTIGATIONS

Single-Mode Theory

The single-mode study was completed with the construction of a nonlinear stability map for the first radial mode. This map is shown in Fig. 8 as lines of constant triggering amplitude (broken lines) and lines of constant limit-cycle amplitude (solid lines) plotted on an $(n,\bar{\tau})$ plane. For each line the value of the peak-to-peak wall pressure amplitude is given. The envelope of all of the constant-amplitude lines is the nonlinear stability limit (not shown for clarity). Triggered instability is possible in the region between the linear and nonlinear stability limits, while the region below the nonlinear stability limit is dynamically stable. This figure shows that triggered 1R instability is more likely to occur for larger values of $\bar{\tau}$. For sufficiently large amplitudes the theory predicts "negative" absolute pressure, thus the theory cannot predict the limit-cycle amplitude of 1R instability for values of n and $\bar{\tau}$ lying to the right of the curve labeled $p'_{min} = -1.0$ in Fig. 8.

Multi-Mode Theory

During the previous report period, a new method of approach to the third order multi-mode theory was developed[2]. Using specific volume instead of density, as one of the dependent variables, the governing system of equations (Equations 21-25 of Ref. 2) were derived. A computational scheme, similar to that described in Ref. 1, was developed. To check out this program, solutions were computed using a series consisting only of the 1-T mode. These solutions (i.e., limit-cycle amplitudes) were compared with previous solutions obtained with available single-mode third order theory obtained with density as one of the dependent variables. This comparison is presented in Fig. 9, for $\bar{\tau} = 1.5$ and $\bar{\tau} = 1.70629$, which shows good agreement between the two approaches. However, due to the approximate nature of the Galerkin method and the difference between the computational schemes for the two cases, exact agreement was not expected.

After this check-out, solutions were obtained with the third order multi-mode program using a three mode series consisting of the 1T, 2T and 1R modes. Limit-cycle amplitudes thus obtained are shown in Fig. 10 where they are compared with similar results obtained with the second order potential theory[1]. These results show that a somewhat smaller limit-cycle amplitude is predicted when third order nonlinearities are included in the analysis.

Some limit-cycle pressure amplitudes for spinning modes were also obtained using a series consisting of the 1T, 2T and 1R modes. These results were compared with the previous results obtained for the standing mode oscillations. This comparison is shown in Fig. 11 for $\bar{\tau} = 1.5$ and $\bar{\tau} = 1.70629$. It is seen that for a given value of $\bar{\tau}$ and a given value of δ (or n), the limit cycle pressure amplitude is higher for a spinning mode than for the corresponding standing mode. This result is in agreement with results obtained with the second order potential theory[1].

Some parametric studies were conducted with the third order theory. First, the variation of the limit-cycle pressure amplitude with the Mach number at nozzle entrance, $\bar{u}_e$, for particular values of n and $\bar{\tau}$ was determined. The third order results for n = 0.61817 ; $\bar{\tau}$ = 1.5 are compared to results obtained for the same value of n and $\bar{\tau}$ using the second order theory (see Fig. 12). It is seen that, for a given value of $\bar{u}_e$, the smaller limit-cycle pressure amplitude is obtained with the third order theory. A similar study involving the chamber length-to-radius ratio, z_e, was conducted and the results are shown in Fig. 13 for three values of n and $\bar{\tau}$. In all three cases, the limit-cycle pressure amplitude was seen to approach a constant value as z_e became large. A similar result was obtained with the second order potential theory[1].

A study of the triggering limits using the third order multi-mode theory is now in progress.

NONLINEAR AXIAL INSTABILITY

During this report period the longitudinal combustion instability investigation consisted of two programs. The first program was concerned with the development of engineering applications of the solutions generated in the second order analysis of moderate amplitude instabilities. The second, and more extensive, program involved the derivation of solution techniques capable of describing the behavior of large amplitude instabilities.

Second Order Analysis: Engineering Applications

The development of the second order (i.e., moderate amplitude) combustion instability solutions is discussed in Ref. 2. In this solution technique, the modified Galerkin method[3] is used to find approximate solutions of a nonlinear wave equation that describes the behavior of moderate amplitude instabilities in rocket combustors having a low Mach number mean flow and a quasi-steady short nozzle.

Correlation with Experimental Data. The results of this analysis demonstrated that the pressure waveforms exhibit a characteristic dependence upon the engine operating conditions. Specifically, the pressure waveforms are dependent upon the proximity of the operating point to engine resonant conditions (i.e., to n_{min} and $\bar{\tau}_{min}$). The observed behavior of the stable limit cycle pressure oscillations can be used to correlate the analytical results with experimental data. To accomplish this task, two waveform parameters are defined in Fig. 14. In this figure, the solid line shows the numerically computed pressure waveform, and the broken line is the theoretical pressure waveform used to determine the correlation parameters $\Delta p'_{max}(z_r)$ and $t_o/T(z_r)$. The normalized axial location at which the experimental pressure data is available is $z = z_r$.

Once z_r is specified, the analytical solution technique developed in Ref. 2 is used to generate both a limit-cycle amplitude map showing curves of constant peak-to-peak pressure, $\Delta p'_{max}$, and a plot of t_o/T as a function of $\bar{\tau}$. Typical graphs, for $z_r = 0.0$, are presented in Figs. 15 and 16. The value of t_o/T can be determined from experimental data. The computed value may then be used in Fig. 16 to determine the value of $\bar{\tau}$. The determined value of $\bar{\tau}$ together with the experimentally determined value of $\Delta p'_{max}$ can then be used, in Fig. 15, to determine the value of the interaction index, n. This correlation procedure should enable rocket design engineers to determine the n and $\bar{\tau}$ values of various liquid propellant rocket motor designs.

Semi-Empirical Pressure Waveforms. At the suggestion of Dr. R. J. Priem, the feasibility of a semi-empirical method for predicting the pressure waveforms has been explored. The objective of the semi-empirical method is to provide design engineers with a straightforward technique, requiring relatively little computation time, for finding the pressure waveforms.

The semi-empirical correlation method is based on the observation[4] that the velocity potential, Φ, can be approximated, at least for resonant oscillations, by the following series expansion:

$$\Phi = A_1 \sum_{n=1}^{N} n^{-\alpha} \cos(n\omega_1 t)\cos(n\pi z) \tag{29}$$

where A_1, α, and ω_1 are found from computer-generated data. The nonlinear pressure waveform is found from the following nonlinear relationship:

$$p' = \frac{\gamma}{2}\left[\Phi_t(\Phi_t - 2) - \Phi_z(\Phi_z + 2\bar{u})\right] \tag{30}$$

The parameters A_1, α, and ω_1 can be found from computer solutions generated using a five term series expansion for Φ, whereas at least a ten term series is necessary to adequately describe discontinuous waveforms[2]. The computation time is approximately proportional to the square of the number of terms retained in the series expansion. Consequently, the computation time required for the semi-empirical method is much less than that required to solve directly for the pressure waveform using the series containing unknown time-dependent functions.

Semi-empirical pressure waveforms are compared with computer-generated solutions in Fig. 17. Ten terms were retained in Eq. (29) in the computation of the semi-empirical waveforms (i.e., N = 10 in Eq. (29)). It is evident from the data shown in Fig. 17 that the semi-empirical method fails to reproduce the waveforms of off-resonant oscillations. The probable reasons for this failure are:

1. There is a slight phase shift between the various modes at off-resonant conditions.

2. For off-resonant oscillations, the higher harmonics are both frequency and amplitude modulated.
3. For off-resonant oscillations, the higher harmonics may not obey the amplitude power law found by considering the behavior of the first ten mode-amplitude functions.

Large Amplitude Instabilities

An understanding of the effect of large amplitude flow oscillations on the stability of rocket engines is necessary for the investigation of engine triggering. An analysis of large amplitude instabilities in low Mach number mean flows has been conducted[5,6]. In the absence of a proven nonlinear unsteady combustion model, Crocco's linear time-lag theory is used to represent the unsteady combustion process. As a result only gasdynamic nonlinearities are taken into account. In the formulation of the problem it is assumed that terms involving the product of an $O(\bar{u}_e^{\,2})$ quantity with a perturbed flow parameter are negligible. However, terms of the form $\bar{u}_e p'^2$ are retained in the governing equations.

Solution Technique

The equations describing the behavior of large amplitude oscillations in a combustor with low Mach number mean flow have been derived in Ref. 6. The undetermined function version of the Galerkin method is used to find approximate solutions of these equations[5,6]. In this solution technique, both the injector solid wall boundary condition and the quasi-steady short nozzle boundary condition are identically satisfied by the series expansions used to represent the dependent variables.

The application of the Galerkin method reduces the original partial differential equations to a system of quasi-linear ordinary differential equations describing the behavior of the mode-amplitude functions. The resulting ordinary differential equations are numerically integrated using a fourth order Runge-Kutta algorithm that has been modified to account for the presence of a retarded time variable[5,6].

In order to find nonlinear solutions the engine operating conditions (i.e., γ, $\bar{u}_e$, $\hat{n}$ and $\hat{\tau}$) and the initial conditions must be specified. The solutions have been found to be dependent upon the engine operating conditions, and independent of the initial conditions.

Convergence Study. In order to minimize the computational time required to find nonlinear solutions, it is desirable to retain as few terms as possible in the series expansions of the dependent variables. A convergence test, in which solutions were generated for five, seven, and ten term expansions, was conducted. The results of this study are summarized in Fig. 18. The convergence of the solutions with increasing number of terms is evident in this figure. The data shown in Fig. 18 also indicates that the behavior of the nonlinear oscillations can be investigated using five term series expansions. The use of five term expansions in lieu of ten term expansions results in approximately a five fold reduction in computation time. Consequently, five term series expansions were used to generate the data discussed in this report.

Results. A comparison of the results of the present investigation with second order solutions computed in Reference 2 is made in Fig. 19. These data show that, when the engine operating conditions are only moderately unstable, the limit-cycle amplitudes are smaller than those found in the second order analysis. It can be shown that these discrepancies are probably due to the different manner in which the short nozzle boundary condition is treated in the two analyses. From Fig. 19 it is also apparent that for more unstable engine operating conditions, the present analysis predicts peak-to-peak amplitudes that are larger than those resulting from the second order solutions. This result is probably due to the fact that the large amplitude oscillations invalidate the second order analysis.

The presence of large amplitude flow oscillations can broaden the region of unstable engine operation predicted by a linear analysis. This conclusion can be drawn from the data presented in Fig. 20. Here, the peak-to-peak amplitudes of the fundamental mode limit cycle oscillations at neutrally stable (in the linear sense) engine operating conditions are presented as a function of $\bar{\tau}$. For $\bar{\tau} > 2/3$, the higher longitudinal modes are linearly stable along the 1L linear stability limit. Consequently, the finite amplitude oscillations along the 1L linearly stability limit are due to flow nonlinearities.

The behavior of the combustion instability oscillations in the linearly stable region is shown in Fig. 21. In this figure, the limit-cycle peak-to-peak amplitudes are shown as a solid line. The critical flow disturbance required for triggering unstable engine operation in a linearly stable region is shown as a broken line. The data presented in Fig. 21 indicate that the flow nonlinearities only slightly broaden the region of possible unstable engine operation.

For engine operating conditions at which the second axial mode is linearly unstable, the behavior of the combustion instability oscillations predicted by the present analysis is the same as that found in the second order wave equation solutions. That is, when both the 1L and 2L modes are linearly unstable, the instability will be in the 1L mode for engine operating conditions of primary interest (i.e., $\hat{n} < 2.0$). On the other hand, when the 2L mode is linearly unstable while the 1L mode is linearly stable, the flow instability will exhibit 2-L characteristics. Typical flow oscillations are presented in Fig. 22.

Discussion and Conclusions

The data presented in the preceding sections, together with the results discussed in Reference 2, indicate that to second order accuracy, the regions of axially unstable engine operation on the $\hat{n}$-$\bar{\tau}$ stability plane can be predicted by a linear analysis. The presence of large amplitude flow oscillations slightly broadens the region of unstable engine operation. However, because of the extreme narrowness of the nonlinearly unstable regions, they can probably be neglected from a practical point of view.

The results of this investigation indicate that second order solutions adequately describe the behavior of axial mode instabilities over a broad range of engine operating conditions. The second order analysis is considerably simpler than the solution of the equations describing large amplitude oscillations, and the former approach requires significantly less computation time.

It is important to note that these conclusions are based on the use of a linear unsteady combustion model. Such a model, while rigorous to second order, does not include nonlinear unsteady combustion effects which may be important in the presence of large amplitude oscillations.

REFERENCES

1. Powell, E. A. and Zinn, B. T., "The Prediction of the Nonlinear Behavior of Unstable Liquid Rockets," NASA CR-72902, July 1971.

2. Zinn, B. T., Powell, E. A., Lores, M. E., Kalyanasundaram, S., "Application of the Galerkin Method in the Design of Stable Liquid Rocket Motors," Semi-Annual Report of Research Conducted Under NASA Grant NGL 11-002-083 for the period February 1, 1971 to July 31, 1971.

3. Zinn, B. T., and Powell, E. A., "Application of the Galerkin Method in the Solution of Combustion Instability Problems," Proceedings of the 19th Congress of the International Astronautical Federation.

4. Private communication from Dr. R. J. Priem.

5. Lores, M. E., and Zinn, B. T., "Nonlinear Longitudinal Combustion Instability in Liquid Propellant Rocket Engines," to appear as a Contractor Report for NASA Research Grant NGL 11-002-083.

6. Lores, M. E., "A Theoretical Study of Longitudinal Combustion Instability in Liquid Propellant Rocket Engines," Ph.D. Thesis, Georgia Institute of Technology, March, 1972.

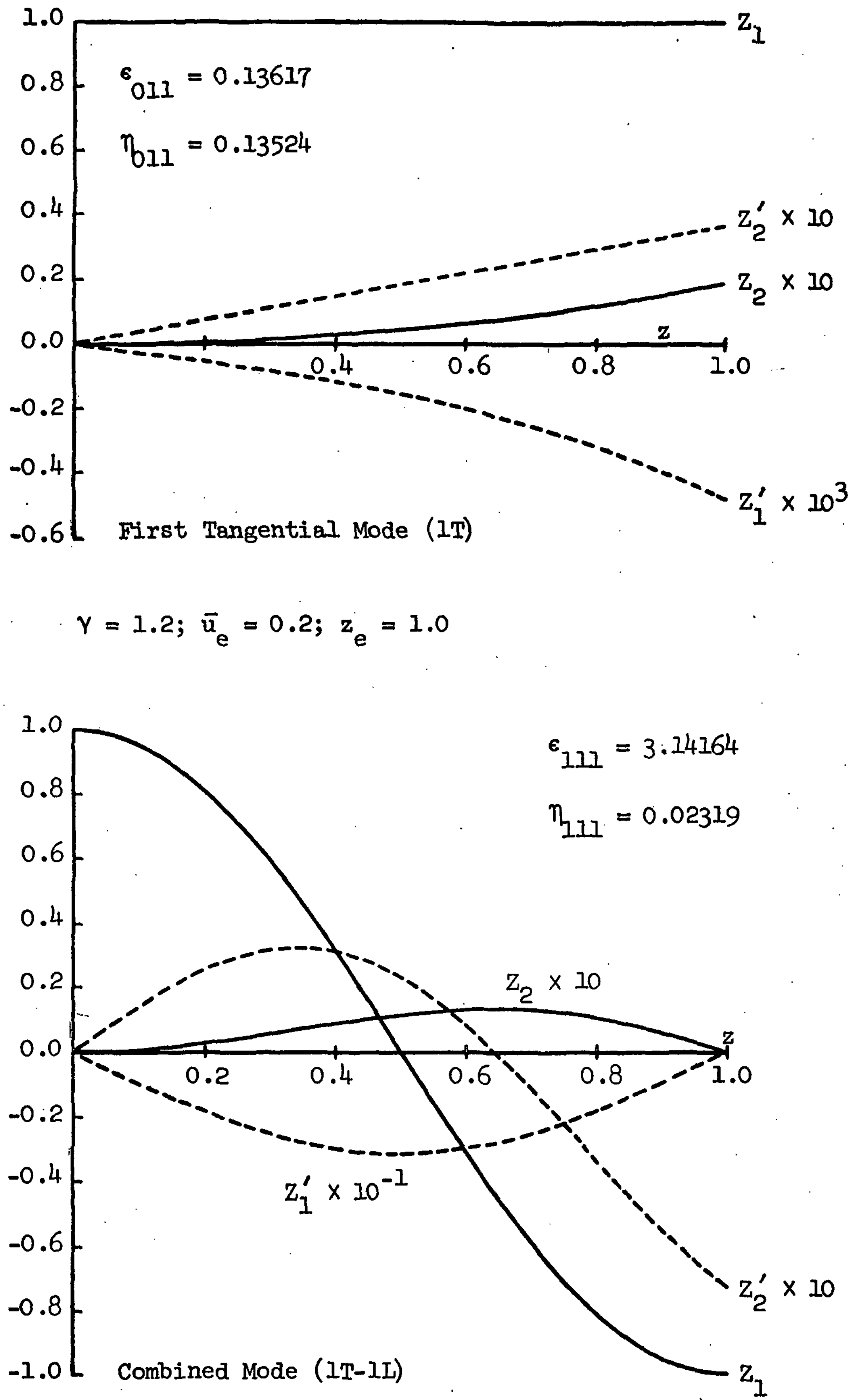

Figure 1. Axial Acoustic Eigenfunctions

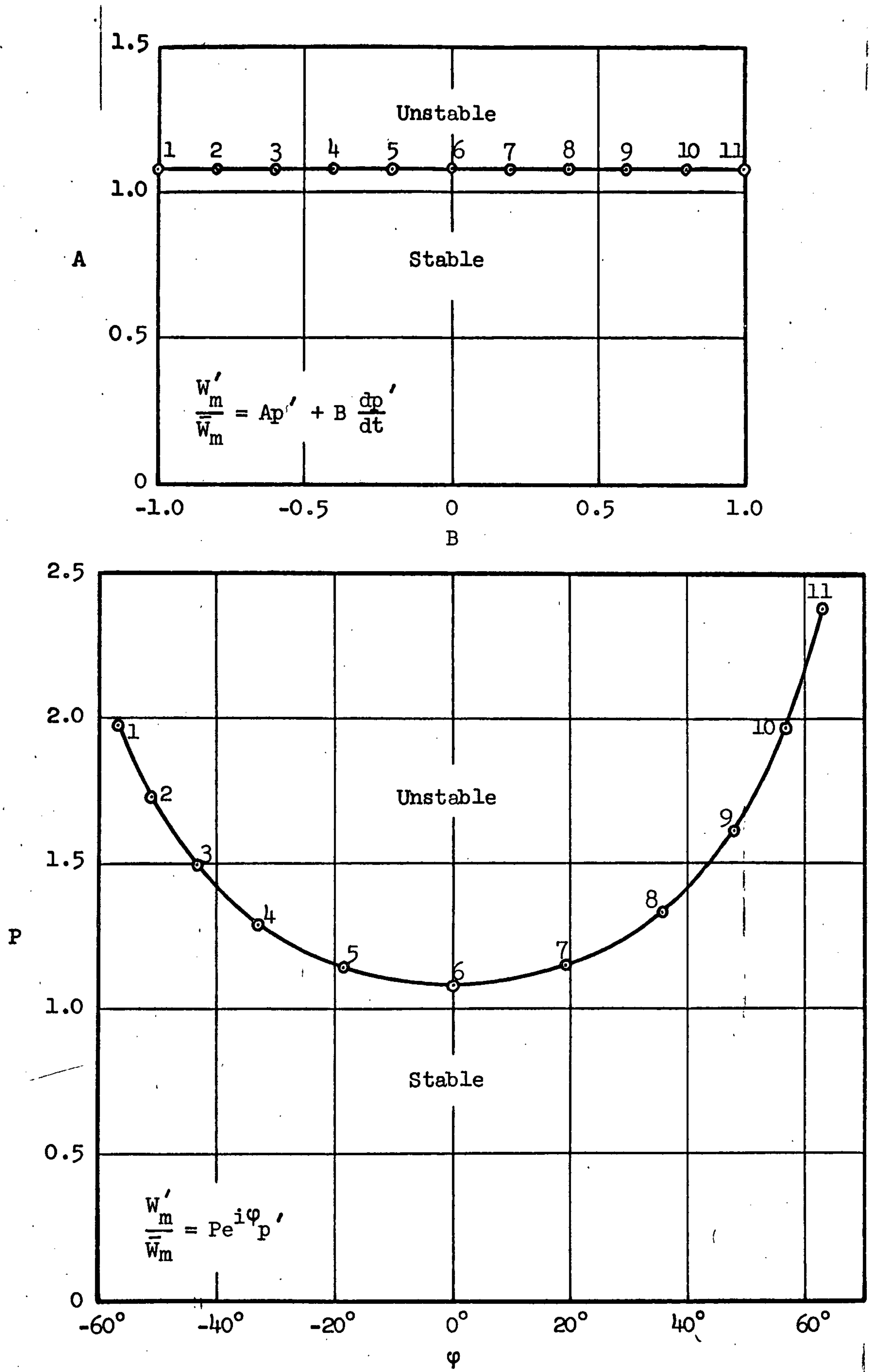

Figure 2. Linear Stability Limits

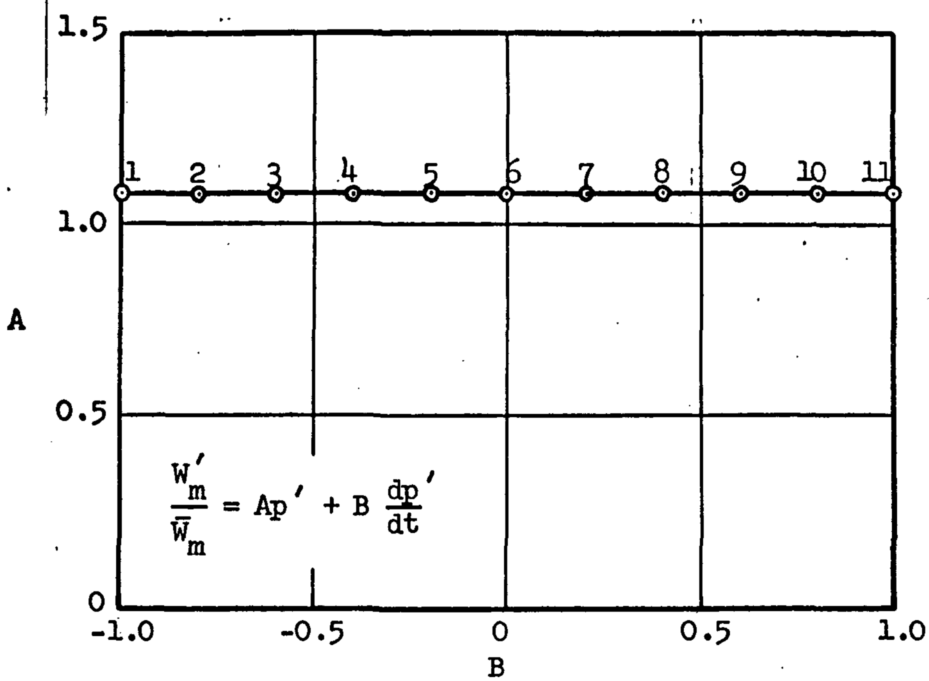

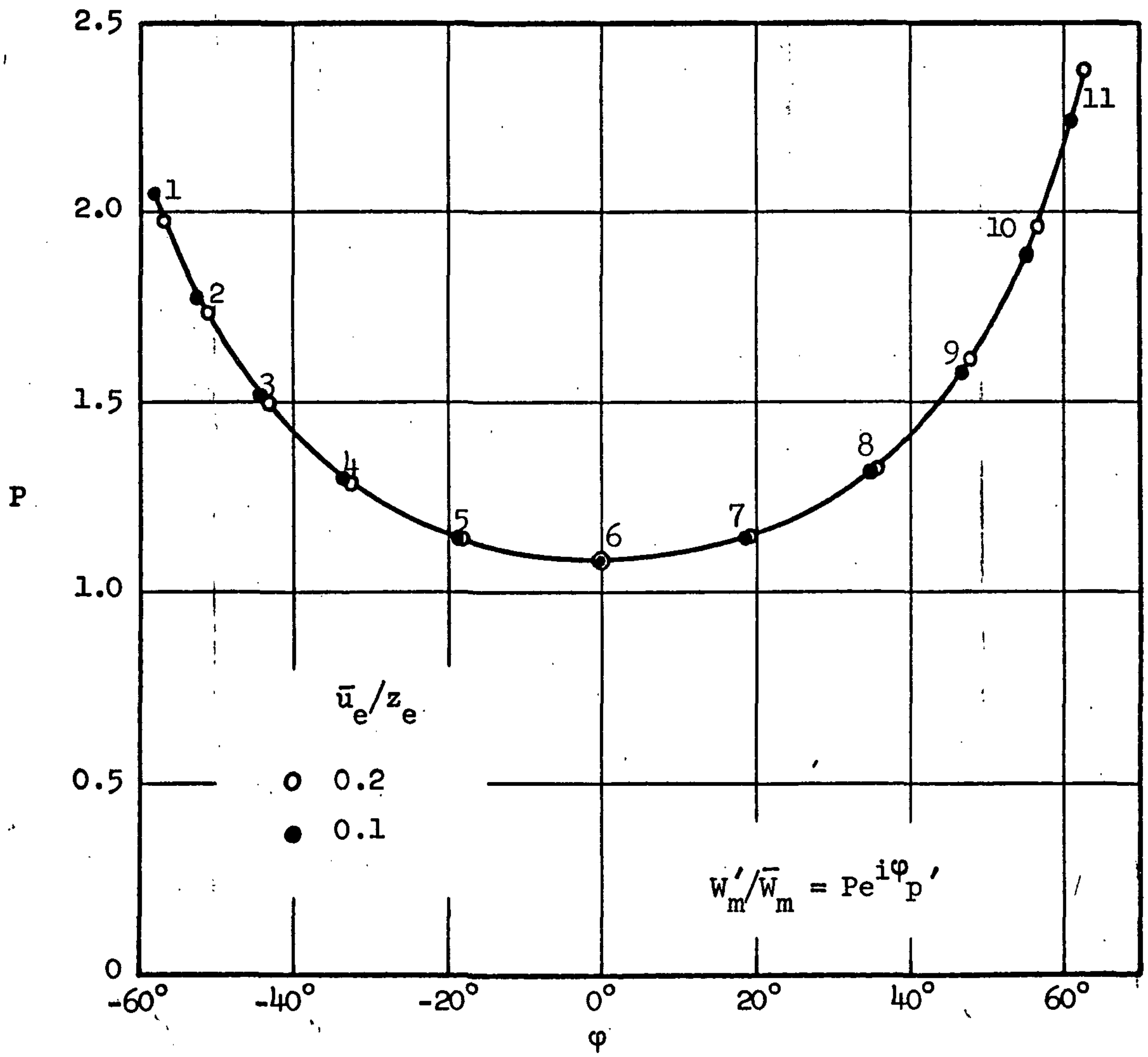

Figure 3. Effect of $\bar{u}_e$ and z_e on Stability Limits

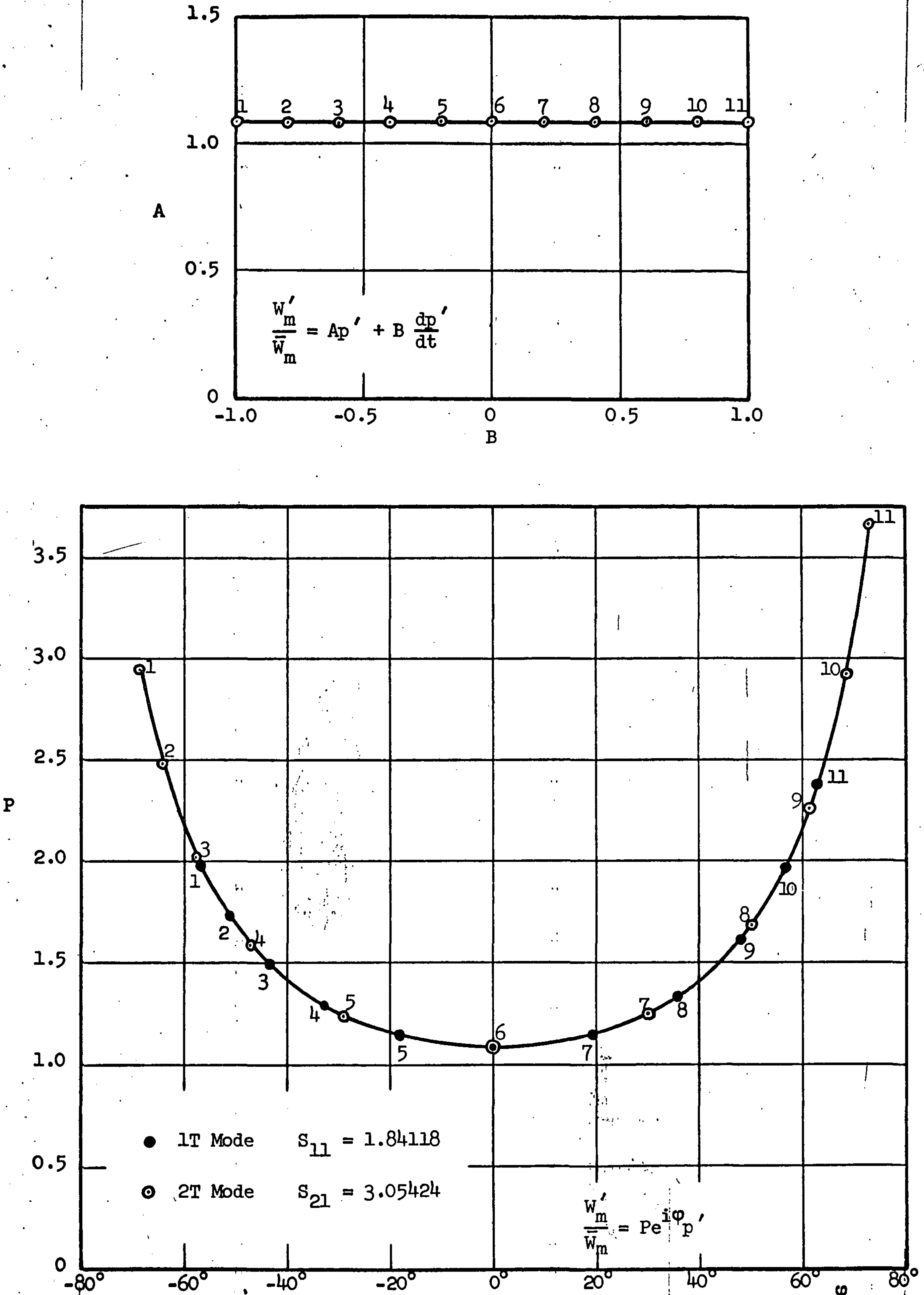

Figure 4. Effect of Mode on Stability Limits

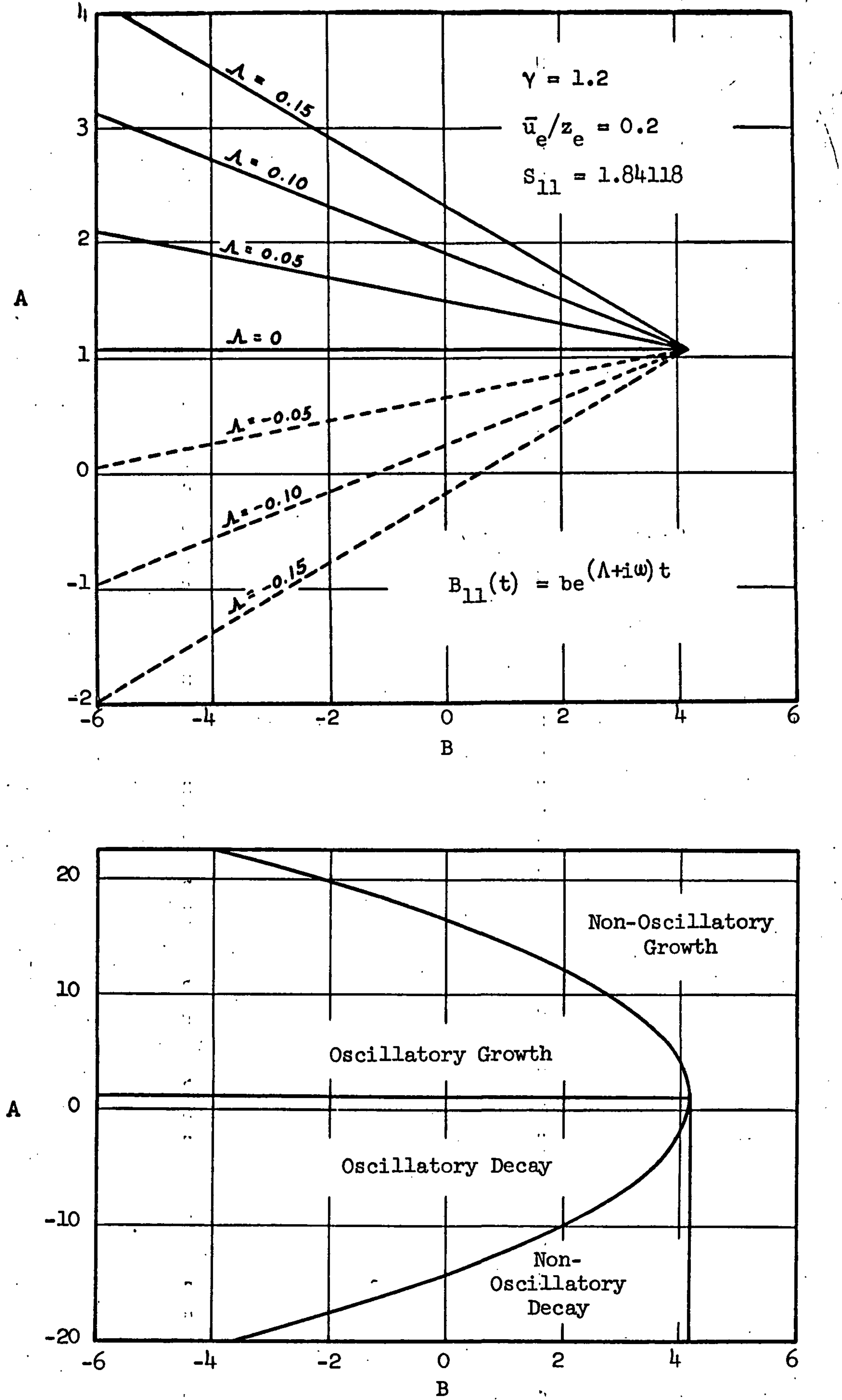

Figure 5. Linear Growth and Decay Characteristics of the 1T Mode

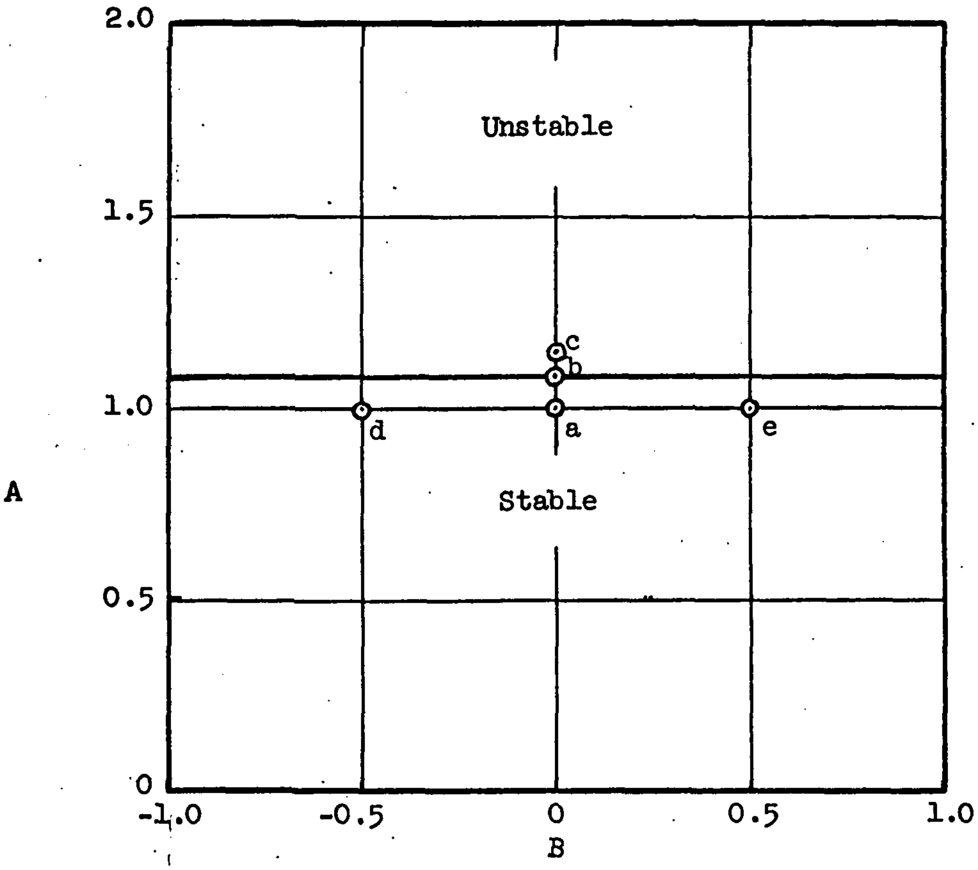

Figure 6. Points Considered in the Nonlinear Study

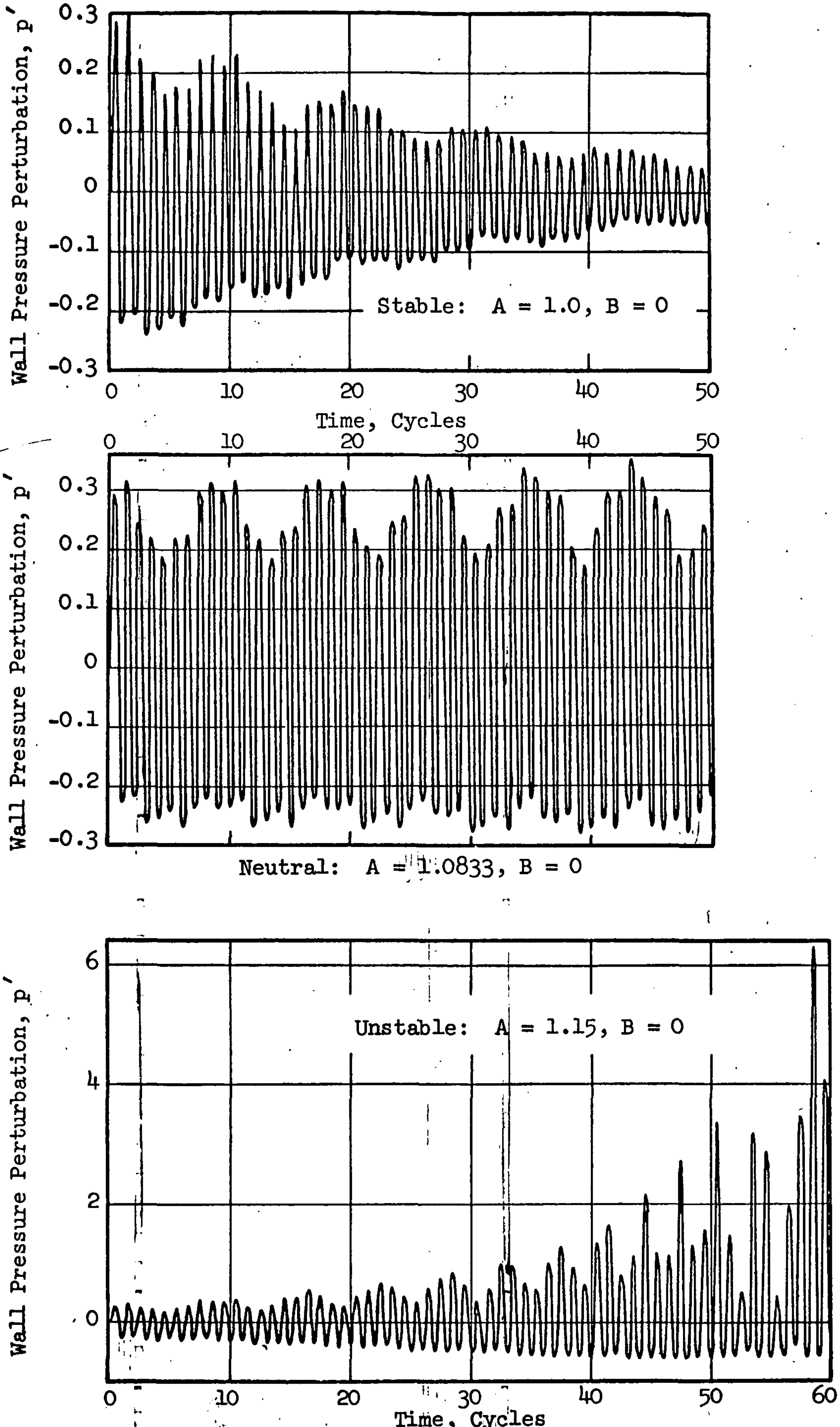

Figure 7. Typical Nonlinear Pressure-Time Histories

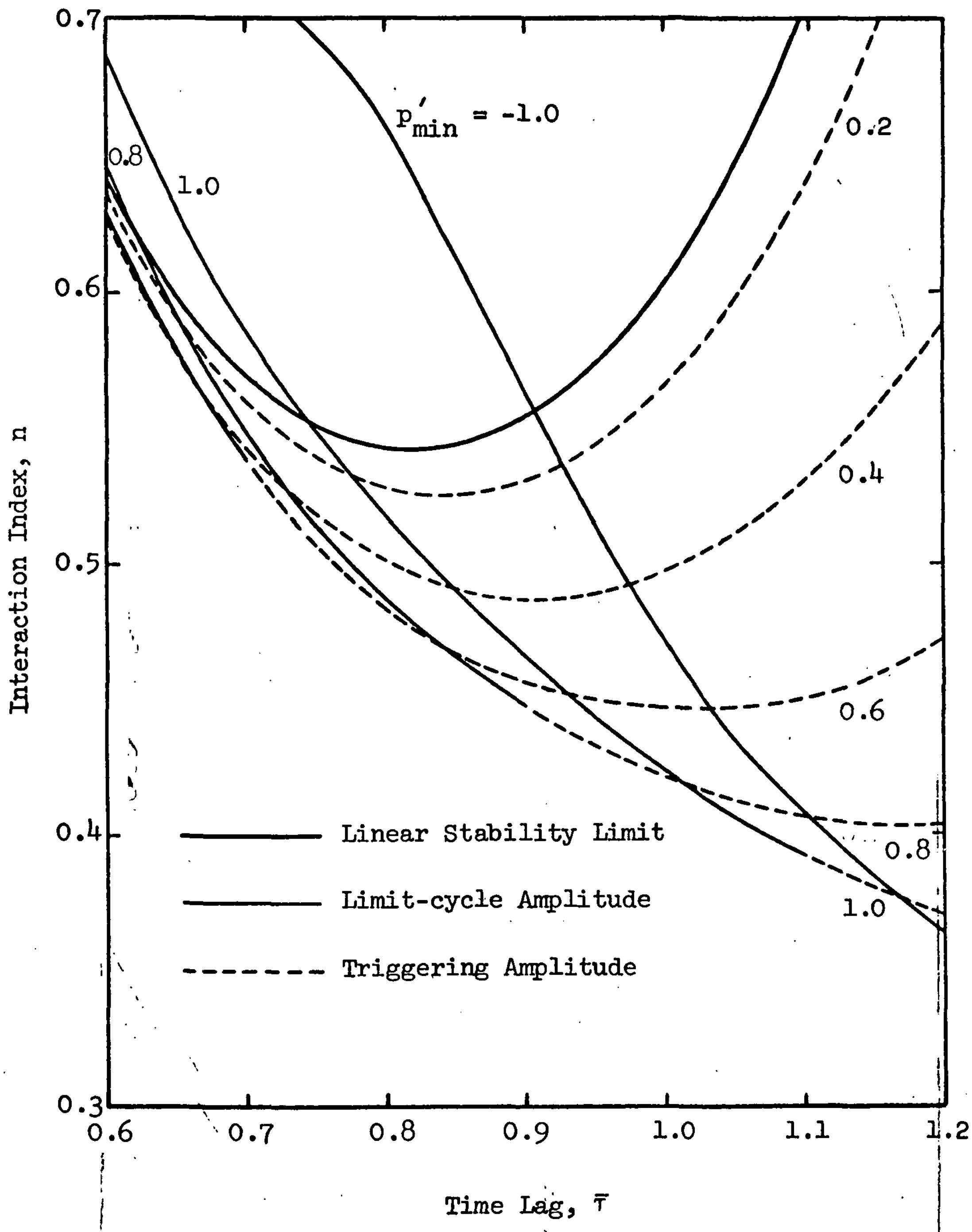

Figure 8. Nonlinear Stability Map for the First Radial Mode

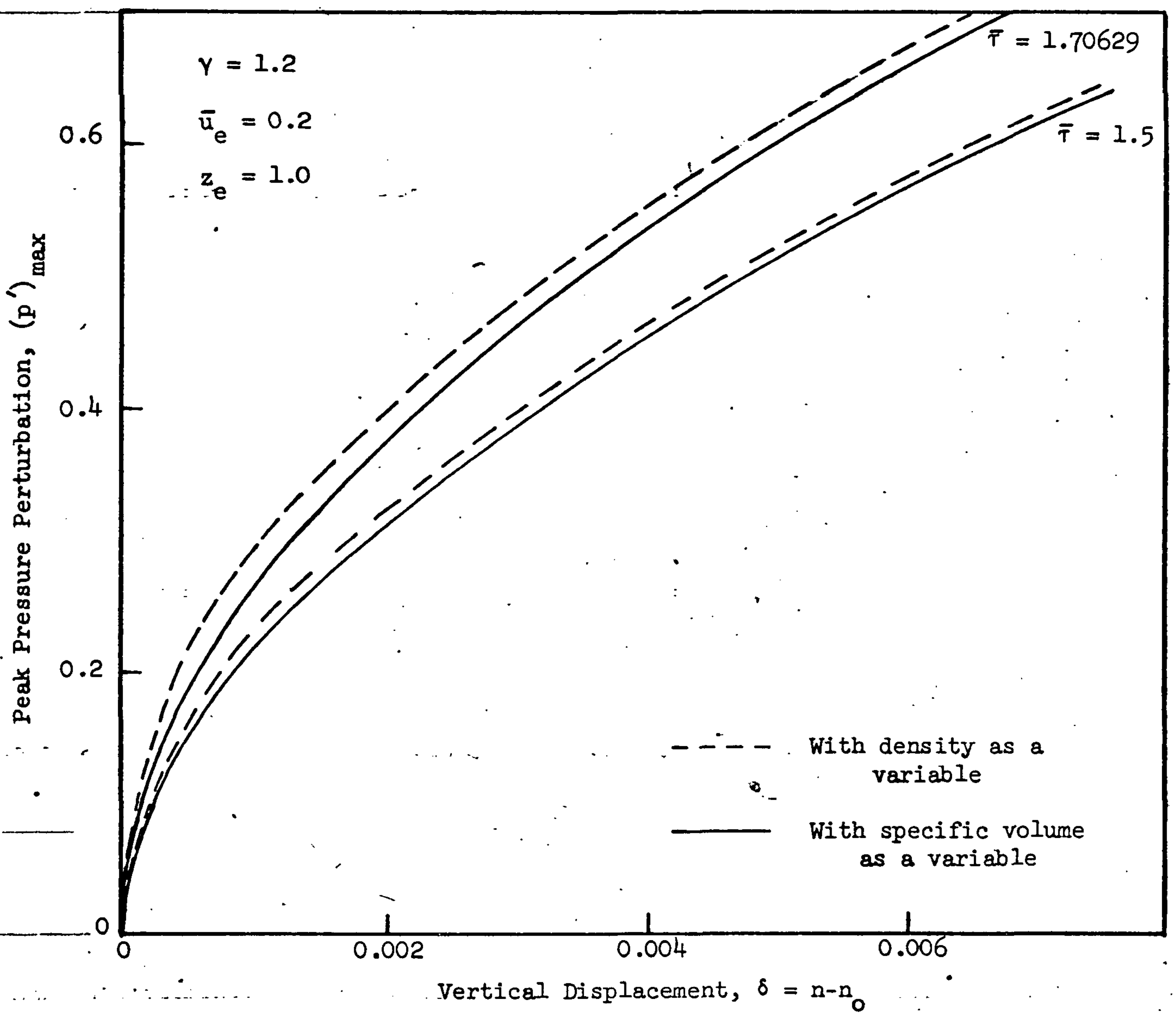

Figure 9. Comparison of Single-Mode (1T) Solutions

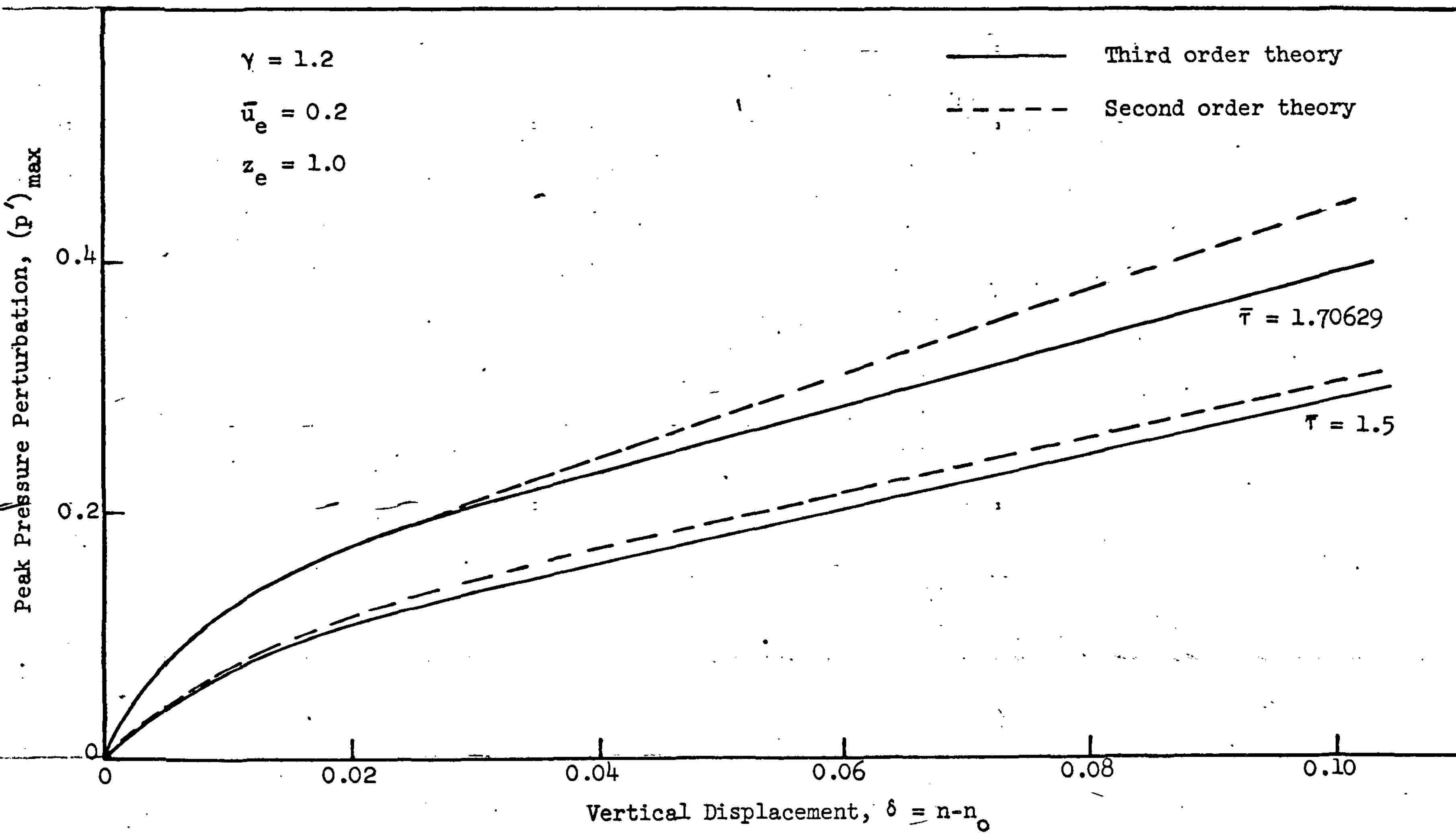

Figure 10. Comparison of Second Order and Third Order Solutions

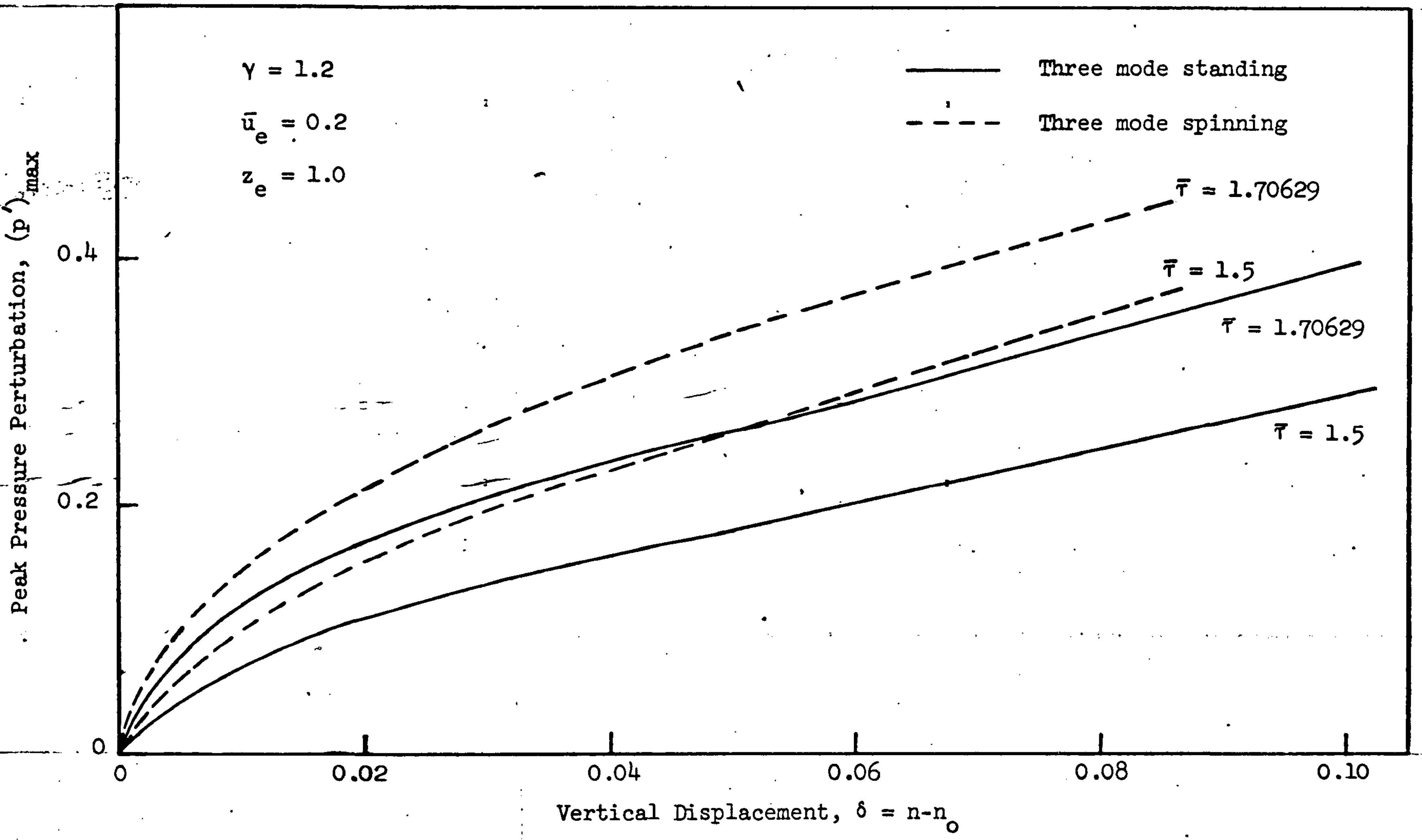

Figure 11. Comparison of Standing and Spinning Third Order Solutions

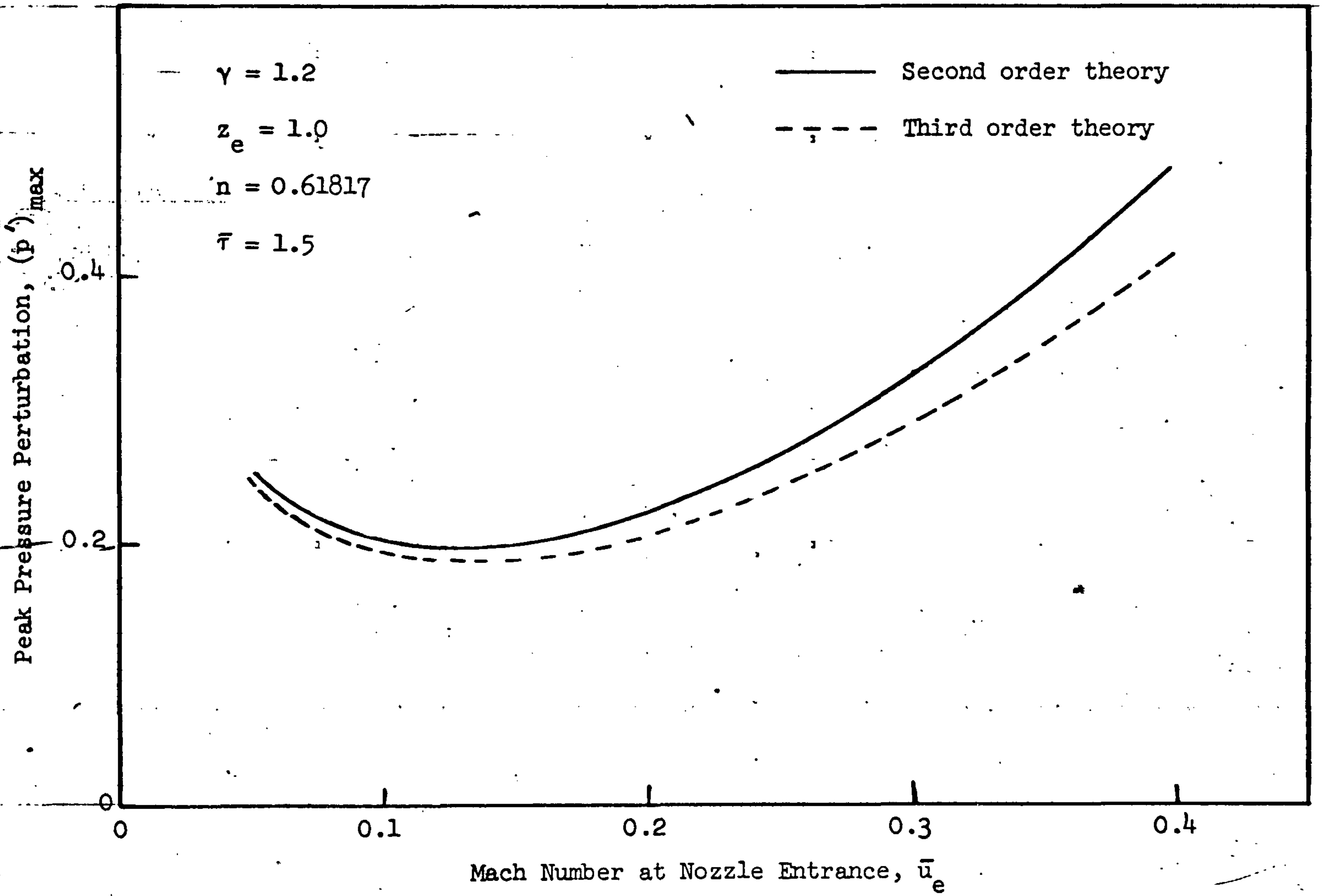

Figure 12. Effect of Chamber Mach Number

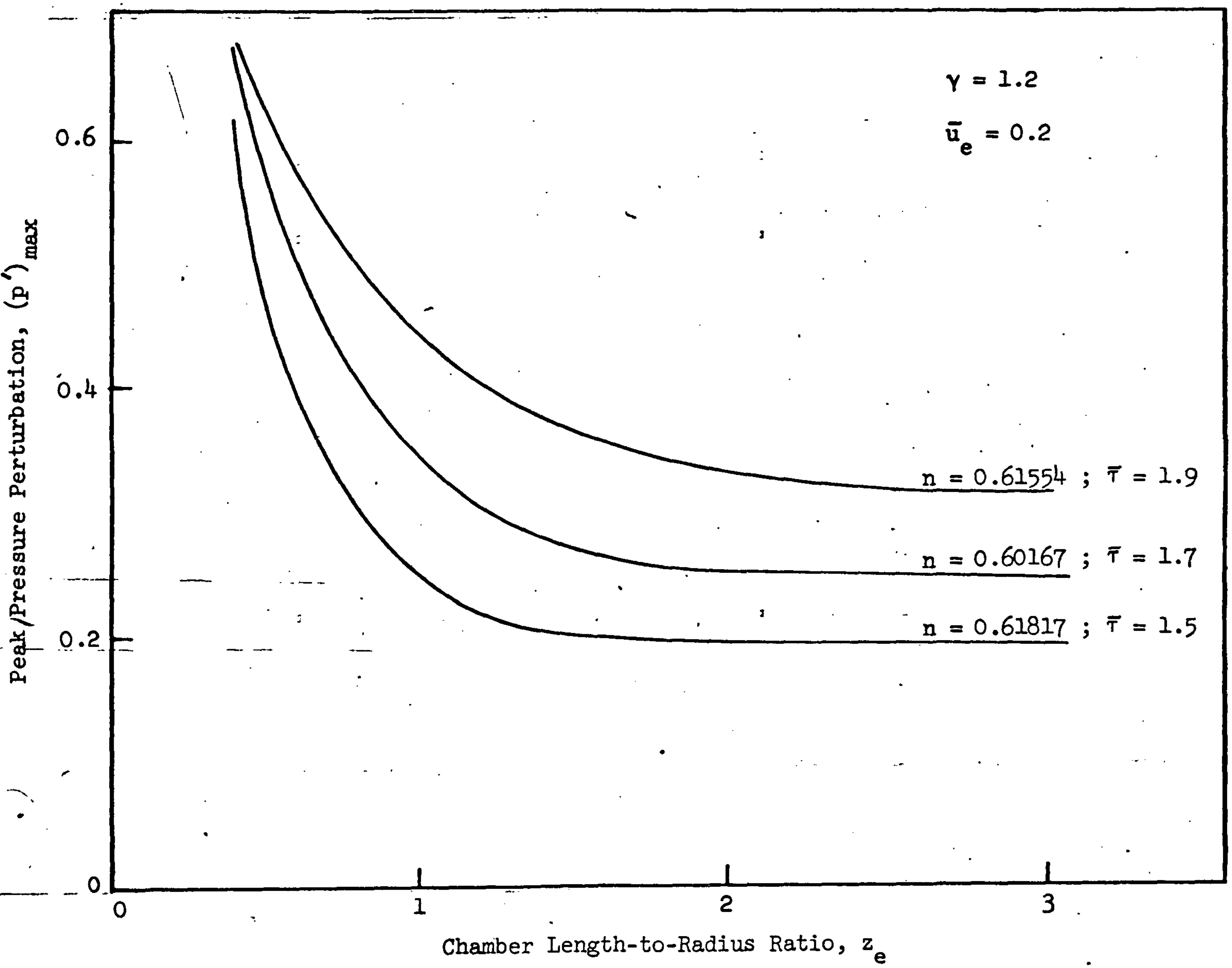

Figure 13. Effect of Chamber Length

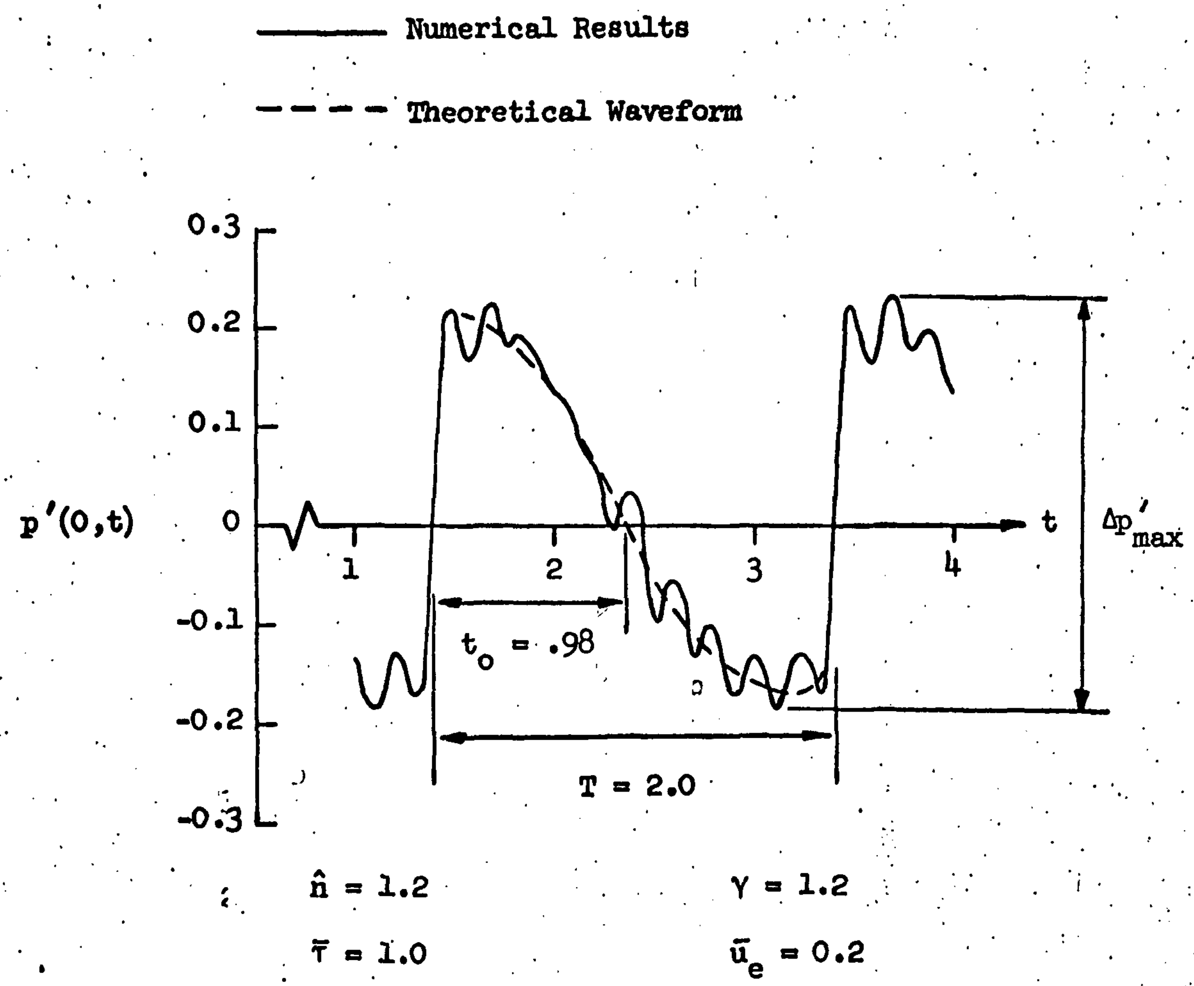

Figure 14. Theoretical Pressure Waveform Used to Determine t_o/T

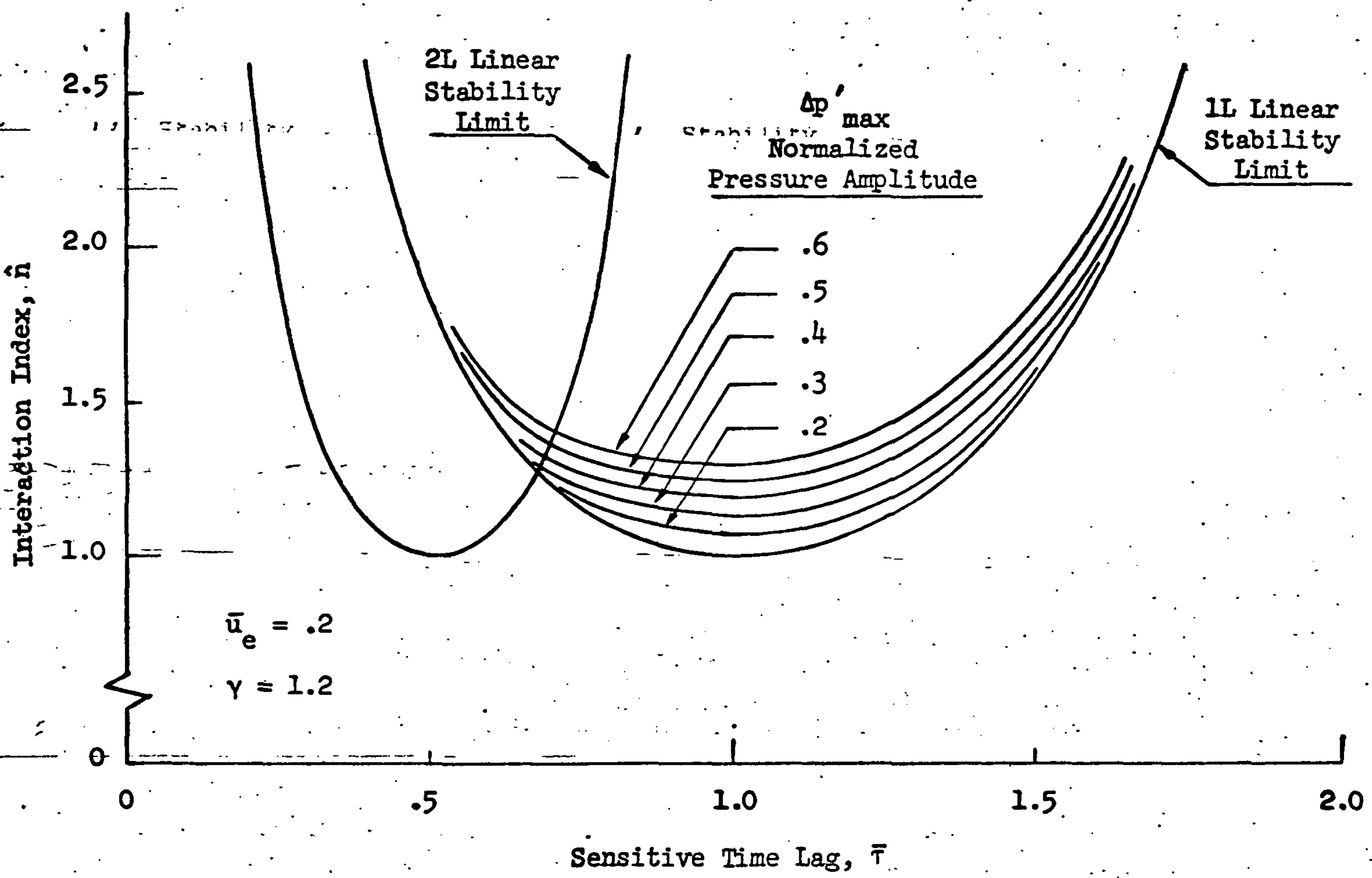

Figure 15. Injector Peak-to-Peak Pressure Amplitudes

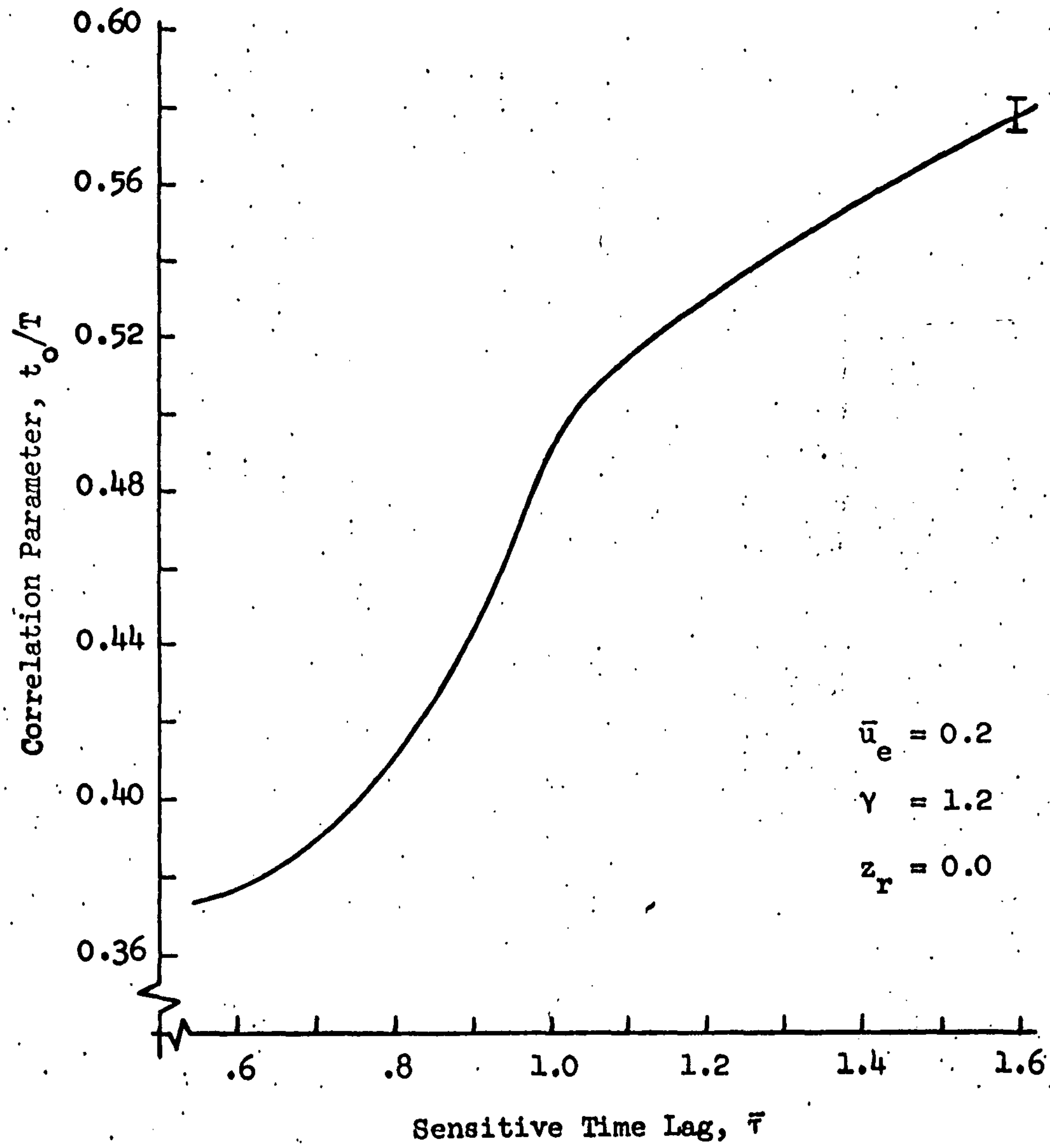

Figure 16. Waveform Correlation Parameter t_o/T

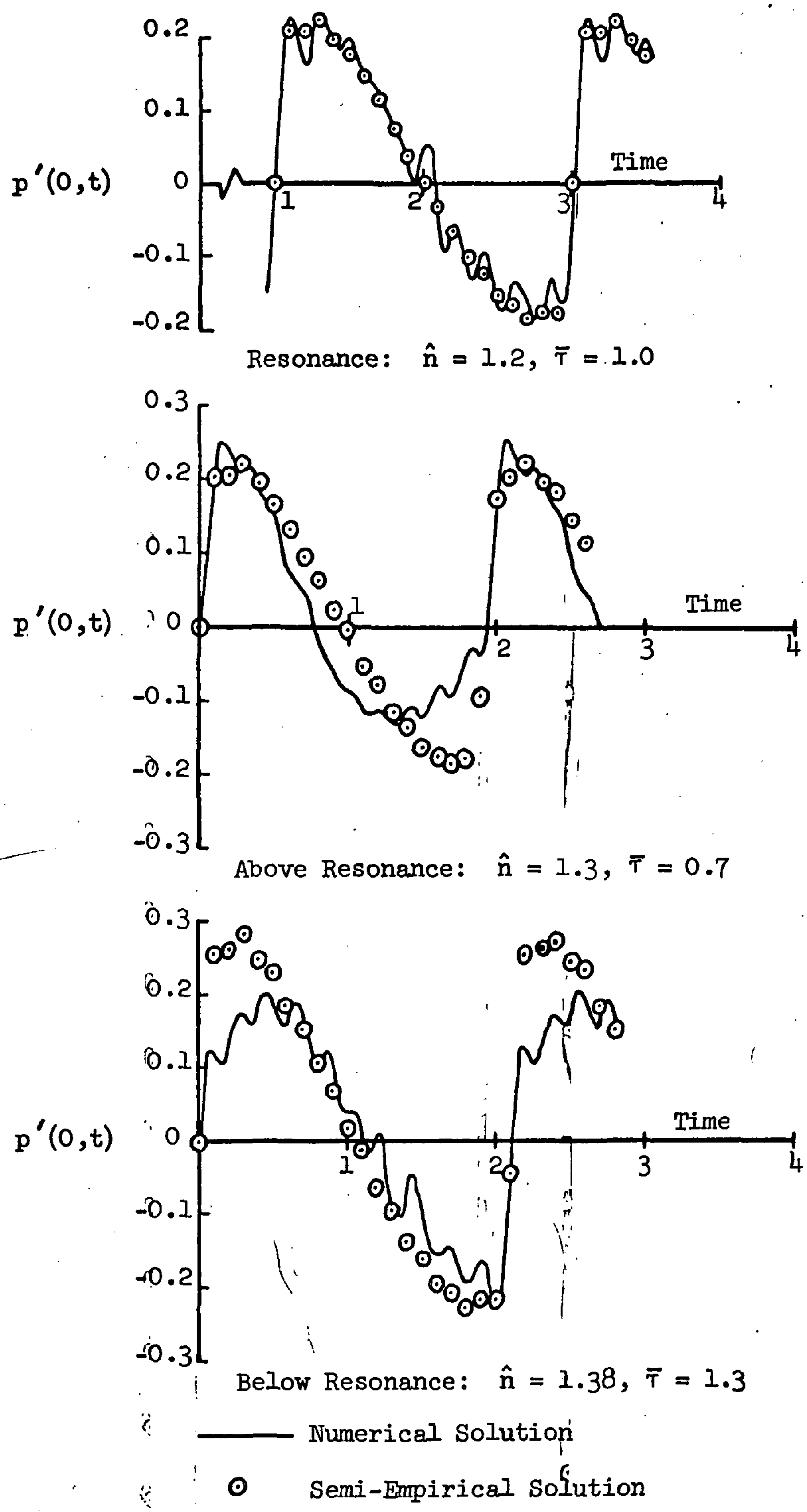

Figure 17. Comparison of Numerical and Semi-Empirical Pressure Waveforms.

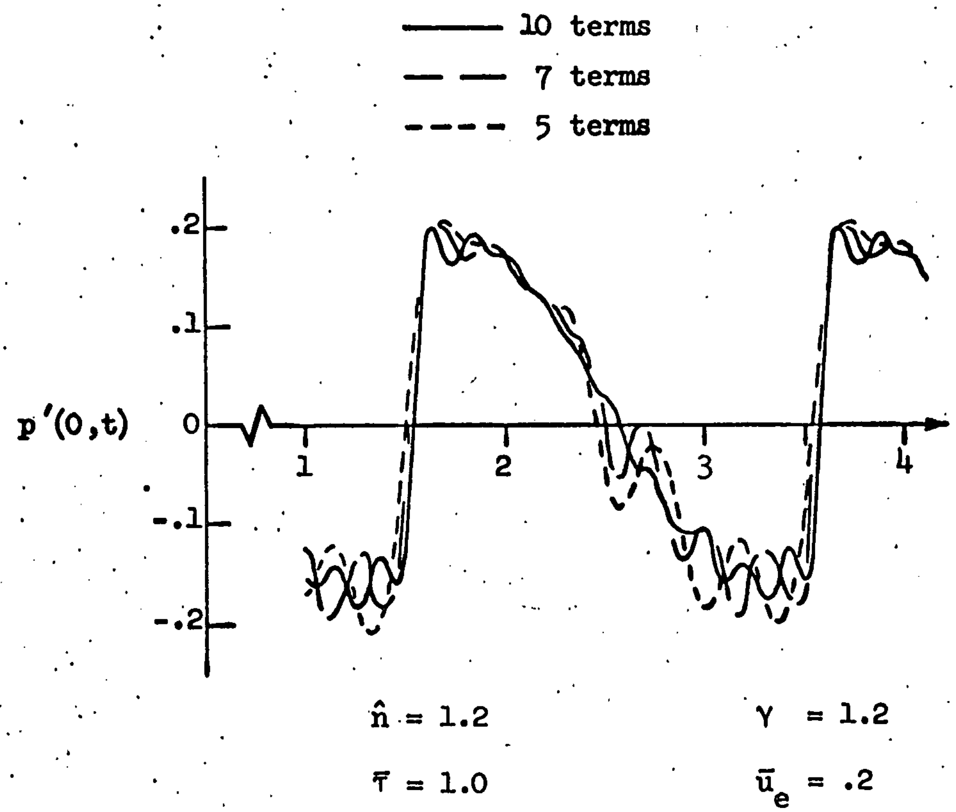

Figure 18. The Effect of the Number of Terms in the Series on the Injector Face Pressure.

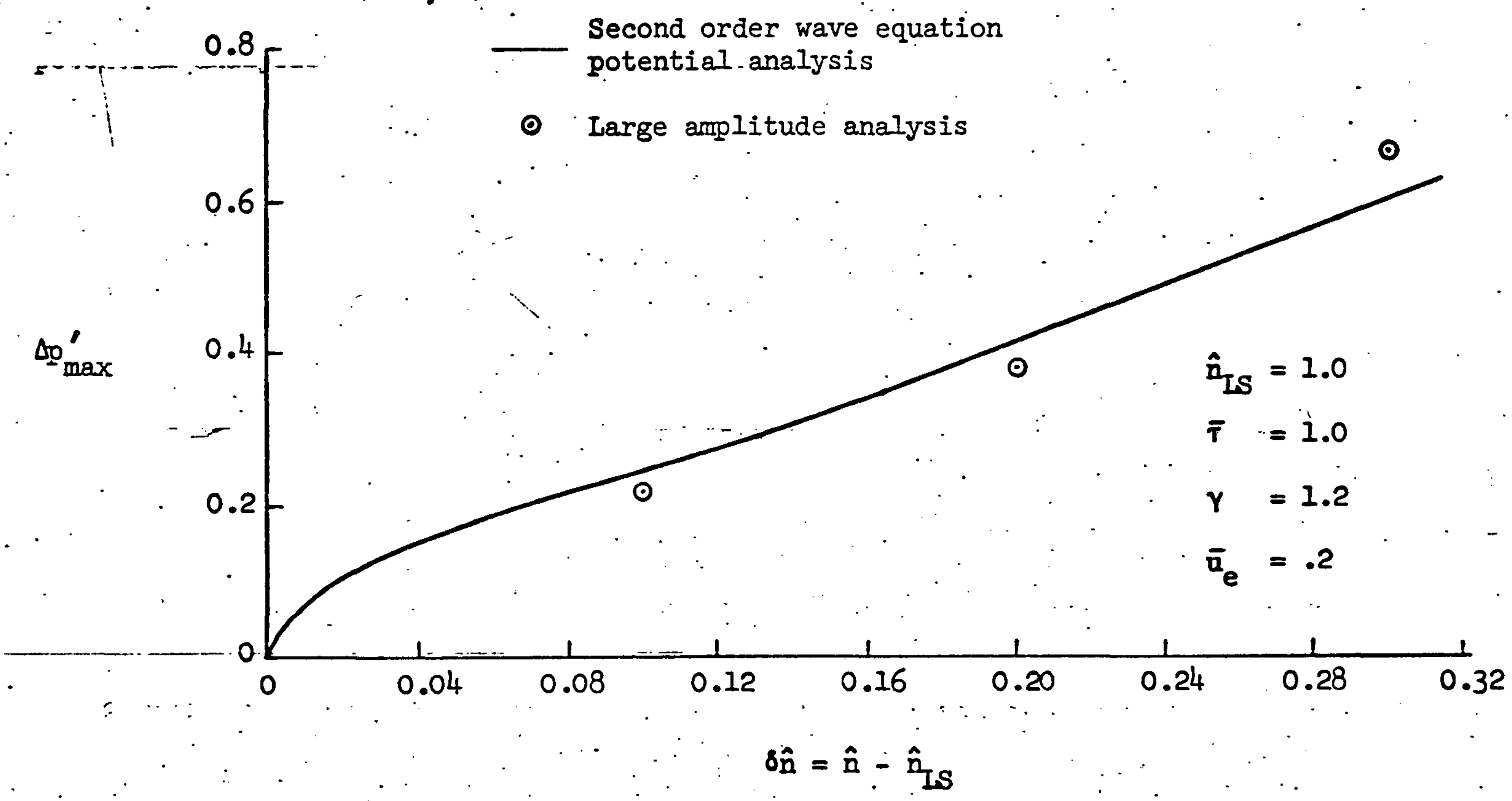

Figure 19.—A Comparison of the Large Amplitude Analysis with Second Order Wave Equation Solutions

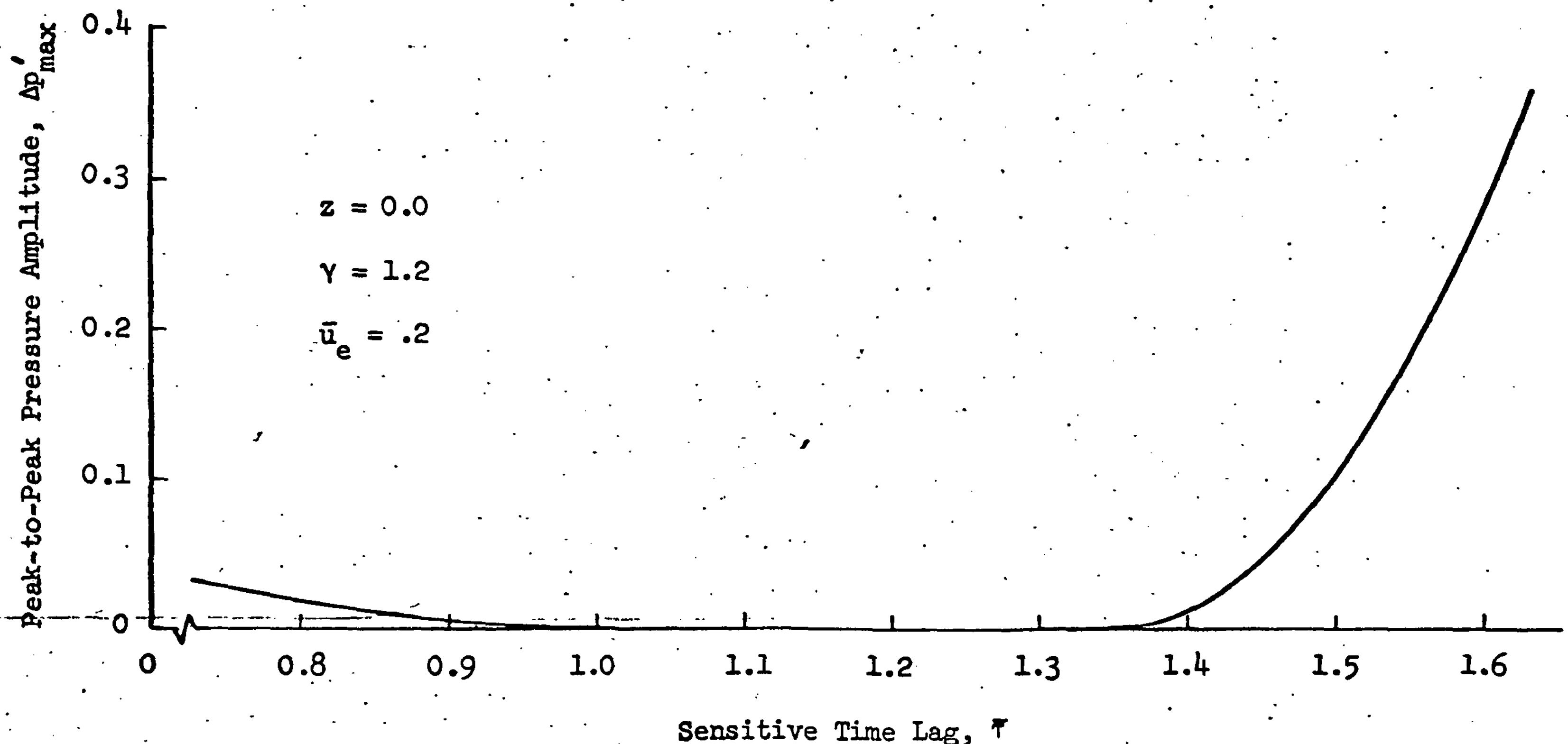

Figure 20. Peak-to-Peak Injector Face Pressure on the Linear Stability Limit

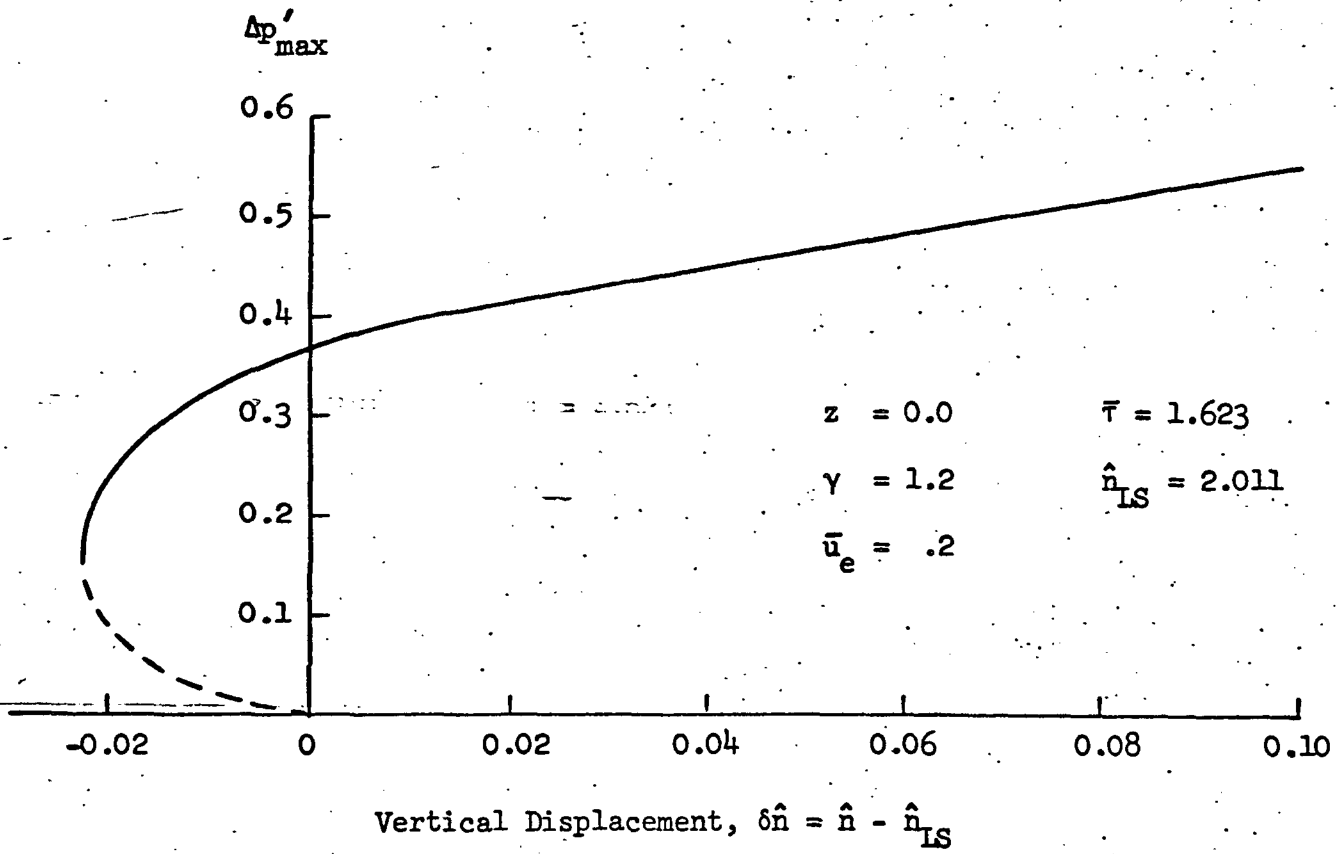

Figure 21. The Effect of Large Amplitude Oscillations on Engine Stability

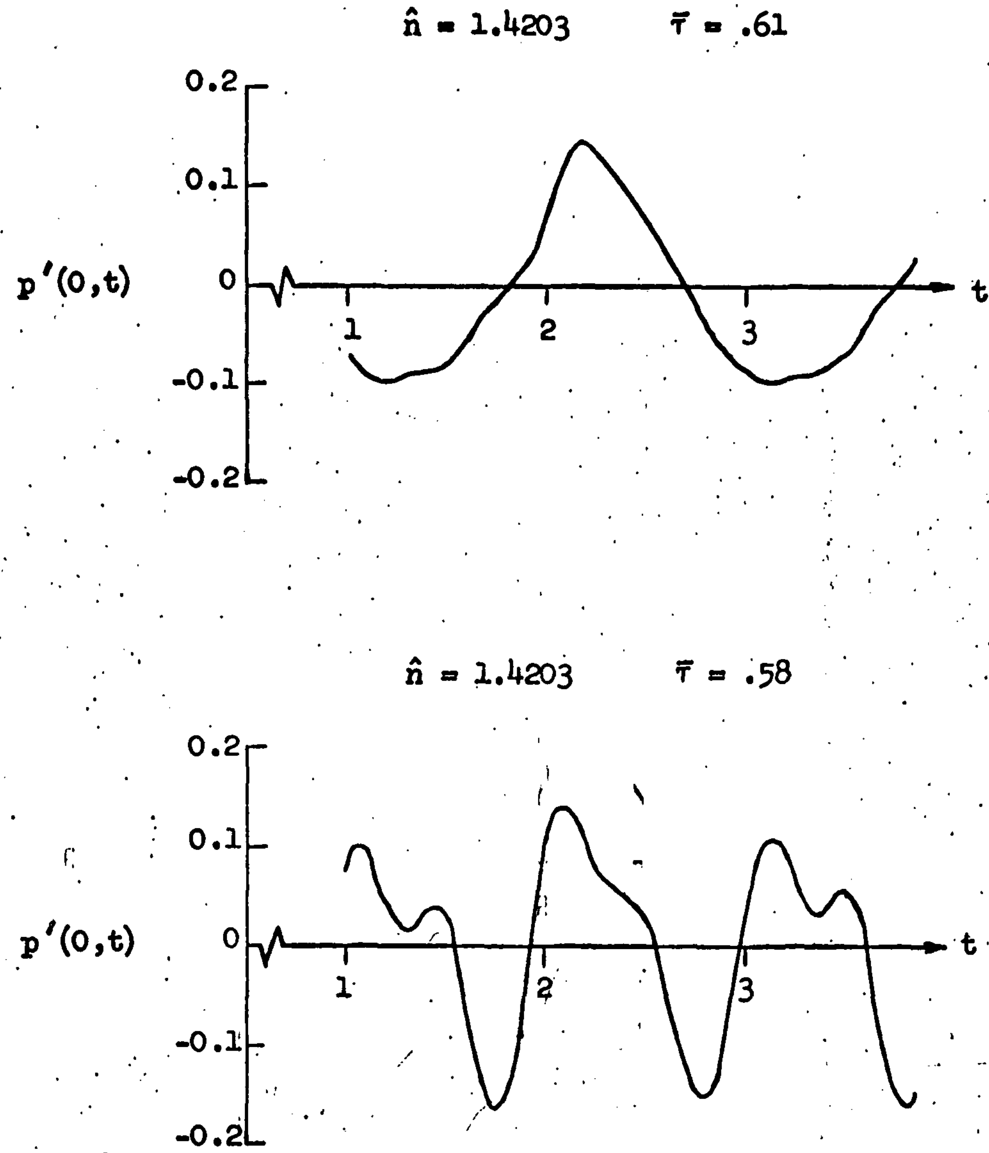

$\hat{n}_{1L} = 1.4203$ $\gamma = 1.2$

$\bar{\tau}_{1L} = .5939$ $\bar{u}_e = .2$

Figure 22. Dependence of Nonlinear Waveforms on $\hat{n}$ and $\bar{\tau}$ (Large Amplitude Analysis)